Cell Power: Quantifying Cellular Forces in 3D Self-Assembled Microtissues

by

Jacquelyn Youssef

B.S., Worcester Polytechnic Institute, 2006

Submitted in partial fulfillment of the requirements for the degree of Doctor of Philosophy in the Program of Biomedical Engineering at Brown University

Providence, Rhode Island

May 2012

This dissertation by Jacquelyn Youssef is accepted in its present form by the Program of Biomedical Engineering as satisfying the dissertation requirement for the degree of Doctor of Philosophy.

Date_____ _____

Jeffrey Morgan, Ph.D., Advisor

Recommended to the Graduate Council

Date_____ _____

Anubhav Tripathi, Ph.D., Reader

Date_____ _____

Vivek Shenoy, Ph.D., Reader

Date_____ _____

Eric Darling, Ph.D., Reader

Date_____ _____

Kristen Billiar, Ph.D., External Reader

Approved by the Graduate Council

Date_____ _____

Peter M. Weber, Dean of the Graduate School

Curriculum Vitae

Jacquelyn Youssef was born at South Shore Hospital in Weymouth, Massachusetts on March 28, 1984 and was raised in Hingham, Massachusetts. She attended Hingham High School where she played field hockey, ran track, and was a state champion lacrosse player. She graduated from Worcester Polytechnic Institute, in 2006 with a B.S. in Biomedical Engineering. At Worcester Polytechnic Institute she gained research experience in the Lab of Dr. Kristen Billiar, who co-advised her senior engineering project with Dr. George Pins. After graduating, Jacquelyn pursued her PhD in Biomedical Engineering at Brown University under the guidance of Dr. Jeffrey Morgan.

Jacquelyn Youssef

BROWN UNIVERSITY, BOX G, PROVIDENCE, RI 02912
CELL: 781.264.4202 • EMAIL: JACQUELYN_YOUSSEF@BROWN.EDU

EDUCATION

Doctor of Philosophy, Biomedical Engineering; August 2011
Brown University, Providence, RI

Bachelor of Science, Biomedical Engineering; May 2006
Worcester Polytechnic Institute, Worcester, MA

HONORS/AFFILIATIONS

- Biomedical Engineering Society, 2005 – 2006, 2010 – Present
- Tau Beta Pi Engineering Honor Society, 2005 – Present
- Provost's Major Qualifying Project Honorary Mention Award, 2006
- High Honors, 2006
- President's Interactive Qualifying Project Award, 2005

RESEARCH INTERESTS

- The cellular self-assembly process
- Mechanobiology and mechanotransduction
- Tissue engineering
- Cell phenotype in response to culture environment
- The role of cell-cell adhesion in physiology and pathology

RELATED EXPERIENCE

Research

Graduate Research Assistant, Department of Molecular Pharmacology, Physiology, and Biotechnology, Brown University, Providence, RI
October 2006 – Present

- Developed and conducted assays to quantify the forces of cellular self assembly
- Quantified the contribution of protein systems to self-assembly
- Investigated the role of heterotypic cell adhesion in force generation and protein expression
- Directed and advised undergraduates

Senior Undergraduate Research Assistant, Department of Biomedical Engineering, WPI, Worcester, MA
August 2004 – May 2006

- Designed and conducted experiments to investigate the effect of stiffness on cell phenotype in three dimensional collagen gels
- Conducted assays to measure the effect of stretch on cellular protein synthesis
- Directed and advised junior undergraduate laboratory assistants

Senior Undergraduate Major Qualifying Project (MQP) Department of Biomedical Engineering, WPI, Worcester, MA
August 2005 – May 2006

- Designed and validated a novel method for studying the combined effect of substrate stiffness and equibiaxial substrate stretch on the phenotype of mammalian cells in a two dimensional environment

Research Experience for Undergraduates (REU), Department of Biomedical Engineering, WPI, Worcester, MA
June 2005 – August 2005

- Designed a novel apparatus to study the effect of stiffness on cell phenotype in a 3D environment
- Mentored middle school females to stimulate their interest in science and technology

Teaching

Teaching Assistant, Department of Molecular Pharmacology, Physiology, and Biotechnology, Brown University, Providence, RI
September 2007 – December 2007

- Taught graduate and undergraduate students various techniques in molecular and cell sciences
- Coordinated and proctored laboratories
- Tutored students
- Revised and updated laboratory protocols

PUBLICATIONS

Youssef J, Nurse AK, Fruend LB, Morgan JR. Quantification of the forces driving self-assembly of three-dimensional microtissues. Proc Natl Acad Sci U S A. doi:1102559108 [pii]10.1073/pnas.1102559108 (2011).

Youssef J, Bao B, Ferruccio T-M, Morgan JR. "Micromolded Nonadhesive Hydrogels for the Self-Assembly of Scaffold-Free 3D Cellular Microtissues" *Methods in Bioengineering 3D Tissue Engineering.* Francois Berthiaume and Jeffrey Morgan. Norwood, MA: Artech House, 2010. P 151-166.

Youssef J, Morgan JR. Self-Assembled Scaffold-Free Three-Dimensional Microtissues for Tissue Repair. Advances in Wound Care. Volume 1 Chapter 75 (2010).

Tejavibulya, N, **Youssef J**, Bao B, Ferruccio T-M, Morgan JR. Directed self-assembly of large scaffold-free multi-cellular honeycomb structures. Biofabrication. (2011). In Press.

Napolitano AP, Dean DM, Man AJ, **Youssef J**, Ho DN, Rago AP, Lech MP, Morgan JR. Scaffold-free three-dimensional cell culture utilizing micromolded nonadhesive hydrogels. Biotechniques. Oct;43(4):494, 496-500 (2007).

Dean DM, Napolitano AP, **Youssef J**, Morgan JR. Rods, tori, and honeycombs: the directed self-assembly of microtissues with prescribed microscale geometries. FASEB J. Dec;21(14):4005-12. Epub 2007 Jul 12 (2007).

Conforte M.L., Mavromatis M., **Youssef J.**, Pins G., Billiar K.L. A Method to Determine the Effect of Stiffness and Stretch on Cell Phenotype. Bioengineering Conference, 2006. Proceedings of the IEEE 32nd Annual Northeast April 2006: 01(02), 79 – 80 (2006).

ABSTRACTS

Youssef J., Morgan J.R. "Scaffold-Free 3D Self-Assembled Microtissues as a Novel Method for Studying Epithelial to Mesenchymal Transition." *Epithelial to Mesenchymal Cell Transition and Epithelial Plasticity Keystone Symposium 2011.*Vancouver, BC.

Youssef J., Morgan J.R. "Human Fibroblasts Generate Ten Times More Power in Mixed Hepatocyte/Fibroblast Microtissues than in Pure Fibroblast Microtissues." *2010 Biomedical Engineering Society Fall Meeting.* Austin, TX.

Morgan, J.R., Tejavibulya, N., **Youssef, J**., Bao, B., Ferruccio, T.M., "Directed Self-Assembly of Large Scaffold-Free Multi-Cellular Honeycomb Structures," *2010 International Conference on Biofabrication*

Youssef J., Nurse A.K., Freund L.B., Morgan J.R. "Cell Power: Quantification of the Forces Driving the Self-Assembly of 3D Microtissues." *2009 Biomedical Engineering Society Fall Meeting*. Pittsburgh, PA.

Dean D.M., Napolitano A.P, **Youssef J**., Rago A., Morgan J.R. "Rods, tori, and honeycombs: the directed self-assembly of microtissues with prescribed microscale geometries." *2007 Biomedical Engineering Society Fall Meeting*. Los Angeles, CA.

Balestrini, J., **Youssef, J**., Billiar, K.L. "Magnitude of Equibiaxial Stretch Modulates Fibroblast Remodeling of Fibrin Gels," 2005 Summer Bioengineering Conference, Vail, Colorado.

Preface and Acknowledgments

First, I would like to thank Professor Jeffrey Morgan for being such an outstanding advisor. These past five years I have come to realize just how exceptional of an advisor he truly is. It is rare to find such an intelligent, creative, thorough, and personable mentor. I am very inspired by not only his ability to tailor his advising to match the needs of his students but also his dedication to each of his students. I am very appreciative of his efforts in directing and supporting me towards becoming an independent researcher. Thank you Jeff.

I would also like that thank my thesis committee for their support, advice, and willingness to aid me in my dissertation. Especially Dr. Kris Billiar, who gave me the opportunity to work in his lab as a junior in college. Along with his graduate students Dr. Jenna Balestrini and Angela Throm, he gave me the support to begin my career in research. The experience I had in his lab really helped me to know that a PhD was something I wanted to pursue. I would also like to thank Dr. Vivek Shenoy and Peng Chen, and Dr. Ben Freund and Dr. Asha Nurse for their collaborations, both of which were pivotal to this dissertation.

My father and my family also deserve a lot of recognition for all of their love and help over the years. My Dad's support (on many levels) has been invaluable. He is a true model of the sacrificial love every parent should have and he is the one who instilled in me and my siblings a strong work ethic and commitment to family. With anything we would do, he would always encourage us to give it our best effort and to just do it right the first time. He has been one of my biggest role models in my life and I try to flatter myself by thinking that I have inherited just a fraction of his ingenuity and integrity.

Baba, thank you for everything. Yvette, Audrey, Anne, Greg, Peter, and Lizzy, you are my best friends and you are so important to me. One of my biggest inspirations has been watching each of your personal and educational successes. You have always been there for me and have helped me tremendously. Thanks guys, I love you.

Most importantly, I would like to thank my husband Brent. He is the biggest blessing in my life and I am so indebted to him for his continual love, support, and companionship. Brent, thank you for always trying to push me to find answers, for listening to endless presentation rehearsals, and for giving me advice on my project. You are everything I could ever hope for in a husband, I love you.

Lastly, I would like to thank all of the administrative staff in the department for helping me throughout the way, especially Carol Folan and Cheryl Pariseau. As well, thank you to all past and present members of the Morgan, Hoffman-Kim, and Mathiowitz laboratories for your company and technical assistance throughout the years.

Table of Contents

Table of Tables

Table of Figures

CHAPTER 1

1. Introduction and Background

Forces are ever-present in the body. Tissues and cells generate and are subject to a number of forces. In the heart, the myocardium is dominated by striated muscle which contracts to pump blood through the body. Heart valve leaflets are exposed to shear stresses as blood flows through the chambers and pressure gradients as the leaflets modulate blood flow. During respiration lung tissue cycles through strained and relaxed states and alveolar experience surface tension which aids in the expulsion of air. Tendons and ligaments are under tension while bones and cartilage are under compression. Whether osmotic pressure, compression, surface tension, contractile/ tensile forces, or shear stresses the body is greatly under the influence of mechanics (1). Mechanics also play a crucial role in the development of these tissues (2). The successful formation of the heart (3, 4), cartilage and bones (5, 6), lungs (7, 8), kidneys (9), brain (10), and blood vessels (11) are all dependent on mechanical forces. In each of these cases, the tissue is subjected to external forces which create a homeostasis in tissue and help to maintain cell phenotype.

In addition to tissues being under external forces, cells are also force generators and these forces have an important role in embryogenesis and morphogenesis. After fertilization, cell division initiates and the cells within the morula compact as daughter cells exert

tension on one another (12, 13). During gastrulation the cells within the blastula exert forces to deform their apical membranes which results in the folding of the blastula and the appearance of the three germ layers (14, 15). As development proceeds, cellular forces shape these layers of the embryo into the head, tail, and organs through actions of pulling, pushing, and bending (15).

The outgrowth of the tissue as well as cell phenotype are thought to be modulated by cellular forces (16). During morphogenesis, cellular contraction leads to epithelial branching in the lungs and in other tissues (8). In addition to organ branching, tension has also been implicated in directing angiogenesis in the developing lungs and in the fusion of tissues that form the spinal column (15, 17). After development, cell-derived tension continues to be important in the function and maintenance of tissues and has implications in disease states.

1.1. Cellular Forces in Wound Healing and Fibrocontractile Disease

The wound healing process is highly dependent on the tension generated by the fibroblast and its activated phenotype, the myofibroblast. When a tissue is injured, the population and proportion of fibroblast-like cells increases within the tissue (18). The fibroblasts are crucial for healing as they differentiate into the myofibroblast, exert tension to close the wound, and release cytokines and collagen I (18-20). In healthy wound healing, these factors result in the creation of a provisional matrix and the closure of the wound. As the process continues, this provisional matrix is then broken down, via the action of matrix metalloproteinases (MMPs), and remodeled into healthy tissue that is similar in architecture and content to the original tissue. After healing, the fibroblast/myofibroblast cells desist in the tissue through the process of apoptosis and the population of epithelial cells returns to normal, thus restoring the function of the parenchyma (20).

However, in pathologic wound healing, the myofibroblast population persists as the functional parenchyma disappears. The myofibroblasts continue to exert tension, release cytokines, and produce extracellular matrix (ECM) components, all of which can result in hypertrophic scaring, stiffening, and fibrosis of the tissue. Fibrosis is a disease that can affect many organs including the liver, kidney, heart, skin, and lungs. At its most advanced stages, it can lead to organ failure or cancer of the affected tissue. Because cellular contractile forces are thought to be a main culprit in this disease, much research has been carried out to determine what causes quiescent fibroblasts to differentiate into the highly contractile and synthetic myofibroblast.

1.1.1. The Myofibroblast

The differentiation of a fibroblast into a myofibroblast is thought to follow a two step process. In this process, a quiescent fibroblast differentiates into a proto-myofibroblast which in turn differentiates into a myofibroblast. A quiescent fibroblast has cortical actin, is not contractile, and has neither focal adhesions nor cellular fibronectin. A proto-myofibroblast, the typical phenotype of a fibroblast that has been cultured *in vitro* on a stiff material (i.e. polystyrene), is marked by having an elongated shape, stress fibers, cellular fibronectin (with variant ED-A domain), and focal adhesions. Unlike the quiescent fibroblast, the proto-myofibroblast is able to generate tension. A myofibroblast differs from a proto-myofibroblast in that it can generate the highest levels of contractile force, has more of both ED-A fibronectin and stress fibers, and large fibronexus adhesion complexes or supermature focal adhesions, which are found *in vivo* or *in vitro*, respectively. In addition, the myofibroblast expresses α-smooth muscle actin (α-SMA) which is the most reliant marker of the myofibroblast phenotype (20).

The factors causing the activation of the fibroblast into a fully differentiated myofibroblast have been the focus of many studies. The differentiation process of a quiescent fibroblast into a proto-myofibroblast is initiated by mechanical tension. When a fibroblast is seeded in/on a stiff matrix (2D or 3D) it will form adhesions and will pull against the rigid substrate. As the cell exerts these traction forces, there is a recruitment and alignment of the actin cytoskeleton resulting in the development of focal adhesions and stress fibers (21-24). These changes in actin arrangement have been demonstrated with fibroblasts and other cell types on many materials including polystyrene,

polyacrylamide gels with different levels of stiffness, and with cells embedded in constrained and free floating collagen gels (25-29). Once a fibroblast is seeded in/on a mechanically stressed or stiff environment, the cell differentiates into a proto-myofibroblast and begins to produce fibronectin. This fibronectin includes an ED-A splice variant which, in addition to continued mechanical stress and transforming growth factor-β1 (TGF-β1), leads to the activation of the proto-myofibroblast into a fully differentiated myofibroblast (30). Although, there are many factors that are crucial to the differentiation process, mechanical tension is the initiator of this process. As such, much research has focused on trying to understand cell-derived forces and its transmission to other cells and surrounding tissue.

1.2. The Role of the Cytoskeleton and Cellular Adhesion

Cellular force generation is highly dependent on both the cytoskeleton and cell adhesion molecules. As the cytoskeleton generates tension, cell adhesion molecules not only anchor the cell to its external environment, but also act as the transmitter and sensor of these forces.

1.2.1. The Cytoskeleton

The cytoskeleton is a complex biopolymer network in the cytoplasm composed of three main components: microtubules, intermediate filaments, and actin filaments. Microtubules are highly conserved hollow fibers formed by the polymerization of alpha and beta tubulin. Microtubules maintain cell shape by resisting compression and also have a role in intracellular transport. Intermediate filaments are cell type dependent proteins which function in a number of tissue specific cellular processes (31, 32). Although these two filaments do aid in force transmission, the actin cytoskeleton is the most crucial to cellular contraction.

1.2.1.1. Actin Microfilaments and Myosin Motors

Actin microfilaments (f-actin) are formed by the polymerization of globular actin (g-actin) into bundles or networks (33). Networks are constructed from short actin filaments found at the cell's leading edge. The polymerization of these networks leads to the protrusion of the cell's edge resulting in the forward motion of a cell during locomotion. Bundles are thick crosslinked actin filaments that are arranged in parallel to one another. These bundles can be located at the cortex of the cell, forming bundles tangent to the

edge of the cell (cortical actin), or can be formed into stress fibers which span the cytoplasm of the cell and intersect the edge of the cell. These stress fibers, which include myosin, are responsible for the force generation within a cell.

Myosin II is the major non-muscle myosin protein responsible for the contraction of a variety of non-muscle cells. Myosin II motors consist of a globular head region, a neck region, which contains both an essential light chain (MLC) and a regulatory chain, and a tail region, which contains a heavy chain. Prior to force generation, the myosin head is tightly bound to the actin filament. ATP then binds to the myosin, which results in the dissociation of the myosin head from the actin. The ATP is then hydrolyzed, leading to the phosphorylation of the myosin head which in itself causes a conformational change in the neck region of the myosin and then results in the binding of the MLC to the actin. While bound to the actin, the MLC remains in its conformational change until the ADP is released and the myosin is dephosphorylated. After dephosphorylation, the myosin returns to its unaltered conformation which leads to the sliding of the actin filament, which is called the power stroke (34). The phosphorylation of myosin II is controlled by two distinct systems: myosin light chain kinase (MLCK) and Rho Kinase (ROCK) (35, 36).

Actomyosin contractility, produced in stress fibers, is the main mechanism for force generation in non-muscle cells. The forces that are generated in the cytoskeleton, through actomyosin coupling, are then transmitted by the cell to its surroundings through cell adhesion molecules. These cell adhesion molecules are transmembrane and as such have

domains located both on the exterior and interior of the cell. The interior domain of the molecule is tethered to the cytoskeleton, and thus aids in cellular contraction.

1.2.2. Cell Adhesion Molecules

Adhesion molecules can be divided into two main categories: cell-ECM and cell-cell adhesion molecules. These molecules are crucial for not only the transmission of forces but also for the sensing of force.

1.2.2.1. Cell-ECM Adhesion Molecules

Integrins are the major transmembrane molecules that attach cells to their surrounding ECM. Integrins are heterodimers with two transmembrane subunits. The integrin's extracellular domain is the domain which recognizes the binding sites on specific proteins such as collagen, laminin, fibronectin, and other proteoglycans. The intracellular domain creates an anchor to the cytoskeleton, creating stability between the cell-matrix adhesion sites.

Through the binding of many integrins to ECM proteins, cells form focal adhesions. These focal adhesions function as a bidirectional communicator between the inside and outside of the cell (37). Through focal adhesions cells sense changes in adhesion, topography, and substrate stiffness, all of which can result in changes in cell shape, spreading, and function (38-40). It was shown that when forces are applied to focal adhesions using optical tweezers, microneedles, or by stretching the substrate on which the cells are seeded, that these force at the adhesion sites are transmitted into the cell

resulting in changes in the cytoskeleton arrangement and in the generation of stress fibers (41-44).

1.2.2.2. Cell-Cell Adhesion Molecules

Cadherins are the major adhesion molecules that form stable cell-cell junctions. Classic cadherins are calcium dependent glycoproteins that have a single transmembrane domain that is bound to the actin cytoskeleton through a complex that contains β-catenin, p120CTN, plakooglobin, and α-catenin. Similar to focal adhesions, cadherins form adherens junctions that are stabilized in the cytoskeleton. As well, like focal adhesions, it has been demonstrated that forces at adherens junctions are transmitted into the cell and that the junction works as a bidirectional communicator in the cell. Specifically, it was shown using mechanical stimulation that when one fibroblast pulls on a second fibroblast that this force results in an influx in calcium and in the reorganization of the cytoskeleton, both of which are implicated in increased actomyosin contractility (45, 46). In addition, it is hypothesized that the adherens junctions that form between myofibroblasts during wound healing, tether stress fibers, leading to the most effective transmission of forces through a wounded tissue (47).

1.3. Methods for Studying Cell Derived Forces

Since contractile forces are implicated in disease states, the activation of fibroblasts, and in many physiological processes, many methods have been developed to quantify cellular contractile forces exerted at focal adhesions and adherens junctions. These methods can be divided into two main categories, contractile force measurements on 2D substrates and contractile force measurements within 3D matrices.

1.3.1. Cellular Force Measurements Using 2D Substrates

In 1980, Harris and colleagues demonstrated that fibroblasts seeded on thin deformable silicone substrates exert enough force to wrinkle the surface of the substrate (28). Harris postulated that the contractile forces generated by the cells could be calculated by examining the substrate deformation and by knowing the mechanical properties of the substrate. However, the wrinkle pattern made by the cells proved to be difficult to quantify and model and so this observation was qualitative in nature. His observation, however, led to the development of many new methods to measure cellular contractile forces.

1.3.1.1. Traction Force Microscopy

After the observations of the cells seeded on deformable substrates, traction force microscopy was developed to quantify the forces exerted by cells on films and gels (48, 49). In traction force microscopy, a flexible polymer film or gel (e.g. polyacylamide) with a well characterized stiffness is created. During the polymerization process,

fluorescently labeled beads are embedded in the top layer of the gel, ECM proteins are crosslinked to the surface of the polymer, and cells are seeded on the polymer. After seeding, the cells adhere to the film, spread, and migrate on the surface. The traction forces exerted by the cells result in a displacement of the fluorescent beads (**Figure 1**). This bead displacement, during locomotion as well as the recoil of the beads (once cells are removed from the substrate via trypsinization), are used to calculate cellular forces.

Using this method, much information has been gathered about the forces exerted by cells on a matrix and cell locomotion. The bead displacement in this assay renders a precise understanding of what parts of a locomoting cell exerts forces with information on the magnitude and direction of these forces. In this method, the stiffness of the polymer, in this case polyacrylamide, can be easily tailed by controlling the proportion of monomer to crosslinker. This is a key feature as many studies have demonstrated that matrix stiffness plays an important role in the traction forces, locomotion, spreading, protein expression, and proliferation of cells (25, 50).

1.3.1.2. Microfabricated Post-Array-Detectors

Microfabricated post-array-detectors (mPADs) have proved very useful for measuring traction forces. Using photolithography and a replica molding process, polydimethylsiloxane (PDMS) is cast to create an array of flexible cylindrical posts with a defined height and radius (52). Proteins are then stamped on the top surface of the cylindrical posts using microcontact printing. Cells are seeded on the tops of the cylindrical posts, after which the cells attach and exert traction forces. These traction

forces result in the deflection of the posts. Using beam theory and knowing the elastic modulus of the PDMS, the cellular contractile forces are calculated from the post deflection (**Figure 1-2**).

Like traction force microscopy, this method allows researchers to acquire detailed information about location, magnitude, and direction of cellular contractile forces. The stiffness of the posts can also be modulated by changing the height and/or the radius of the posts to physiological relevant levels. This is advantageous, because there is no need for chemical modifications to change stiffness allowing for a more controlled study of the effect of stiffness. mPADs can also be used to create a platform with mechanical anisotropies by altering the height, radius, and shape of select posts within an array and thus creating regions with different levels of stiffness. The adhesiveness of the posts to the cells is also easily controlled by protein stamping, making it possible to have more and less adhesive posts within the same array.

1.3.1.3. Cells on Self-Standing Fibers

Another method which uses beam theory was recently developed to measure how cells buckle polymer fibers (53). In this method, a self-standing polymer scaffold is created by filling a UV-curable organic-inorganic pre-polymer resin between two glass plates. To cure the resin into a fiber scaffold, a high repetition rate femtosecond laser beam is passed through the plates at set distances and intervals creating strips of cured polymer. Laser power and duration of irradiation are used to control fiber diameter. After polymerization, uncured resin is washed away, and the top of the fibers is cut from the

glass plate with a laser. Proteins are adsorbed to the surface of the fibers and cells are seeded. Unlike mPADS, in which cells are seeded on the top surface of multiple posts, in this method cells are seeded on the outer surface of a single cylindrical beam. As the cells exert contractile forces, the beam bends in towards the cells and cellular contractile forces are calculated from the deflection and elastic modulus of the scaffold beam (**Figure 1-3**).

Although each of the above mentioned methods have produced useful quantitative data to describe how cells exert traction forces, there are limitations to each of these methods. First, each of these methods only examines contractile forces in 2D. As the cells attach to the polyacrylamide gel, the mPADs, or the scaffold fibers, the cells take on a flat morphology which is very different from the morphology *in vivo*. As well, the contractile forces exerted here are really that of a single cell interacting with an ECM. This lacks the complexity of the *in vivo* environment in which there are multiple cells not only interacting with a matrix, but also with one another in a very intricate fashion.

1.3.2. Cellular Force Measurements Using 3D Matrices

Presenting an alternative to flat 2D substrates, collagen matrices have been used extensively to measure cellular contractile forces. It has long been known that when fibroblasts are seeded within a collagen matrix that the cells will exert contractile forces that bend and buckle the struts of the matrix which results in a remodeling, compaction, and general contraction of the matrix (54). Taking advantage of these phenomena, many assays and devices have been made to quantify cellular contraction in collagen sponges and gels.

1.3.2.1. Bulk Collagen Gel Contraction

Although there are many variations in the methods to measure cellular contraction in collagen gels, the majority follow the setup of having a collagen gel anchored at one of its edges to a polymer that is adhesive to collagen while the rest of the gel remains unattached in a non-adhesive hydrophobic well. The unattached edge of the gel is then tethered to a device used to measure the contraction of the gel. Depending on the assay these measuring devices have included strain gauges (55), force transducers (56), and a deflecting beam with a laser proximity sensor (57).

1.3.2.1.1. Culture Force Monitor

The most published device used to measure cellular contractile forces in collagen gels is the culture force monitor (CFM) developed by Eastwood et al (57-60). The most recent iteration of the device includes a silicone rubber well that acts as a non-adhesive dish. Attached to the edges of the well is a Vyon polymer bar that acts as an anchor to the collagen gel. A collagen/cell suspension is then poured into the silicone well and since the silicone well is non-adhesive to the collagen/cell suspension, as the gel polymerizes it attaches only to the Vyon bars. One of the Vyon bars is firmly clamped to the side of the dish and the other bar is attached to a beryllium-copper (Be-Cu) beam of known stiffness. As the cells within the gel exert forces and remodel the gel, the gel contracts creating a deflection in the Be-Cu beam which is measured by a laser proximity sensor (**Figure 1-4**). Using this device and others, much information has been gathered about the effect of gel compliance, how cellular contractile forces change in anchored compared to free

floating matrices, the role of boundary stiffness in regulating cellular contraction, and the involvement of cellular components in the process (27, 57, 59-61).

1.3.2.1.2. Microfabricated Tissue Gauges

Microfabricated tissue gauges (μTUGs) were developed by Legant et al. to measure cellular contraction in microscale collagen gels (62). Similar to this group's creation of mPADs, the process uses photolithography and replica molding to produce an array of PDMS recesses, each of which contain two rectangular PDMS microcantilevers situated a set distance apart. A collagen/cell suspension is then added to the well and it surrounds both of the microcantilevers (**Figure 1-5**). As the gel polymerizes, it creates a collagen/cell matrix that is wrapped around the cantilevers. Over time, the cells contract the collagen gel which results in a deflection of the cantilevers. Microelectromechanical systems (MEMS) are used to report the forces generated in these PDMS cantilevers.

Collagen gel devices such as the CFM and μTUGs present the advantage over mPADs and traction force microscopy in that they create a 3D environment in which cells interact with a native like ECM. As a result, cells move in all three dimensions, interact with one another, as well as with the matrix, and exhibit a morphology closer to that which is found *in vivo*. However, the major limitation of these methods involves calculating a force per cell value. In these systems, it is assumed that each cell within in the gel is an equal contributor to the force generation and so the total force within the gel is simply divided by the number of seeded cells to render a force/cell value. This may not be very accurate as cells within different areas of the gel may be pulling differently. As well, the

force is measured along one axis, and does not account for the force cancellation of cells pulling in multiple directions. The other major limitation is that these methods can only measure the forces of cells on a matrix and does not consider cell-cell interactions.

1.3.2.2. Single Cell Force Measurements

Addressing the limitation of force per cell measurement in bulk collagen contraction assays, methods were developed to measure the contractile forces of individual cells in 3D matrices (61, 63-64). Roy et al. was one of the first groups to measure individual cellular contractile forces in collagen gels (63). Similar to traction force microscopy, bead markers were embedded within a collagen gel and bead displacement and recoil was measured as cells contracted the gel and as cells were lysed, respectively. In conjunction with information about gel stiffness, these bead displacement values were used to calculate maximum force per cell values. Although this method was able to give force values for individual cells, it presented limitations in that although some cells invaded the collagen gel, the cells were seeded on the surface and thus take on a more flat morphology which is similar to other 2D force measurement methods.

Harley and colleagues also developed a method to measure the contractile forces of individual cells within a collagen gel (64). In this method, the matrices are modeled as a tetrakaidecahedron unit cell with each edge of the unit cell a strut within the collagen matrix. The matrices were seeded with cells at a low seeding density so that the majority of the struts was only surrounded by a single cell. Matrices were imaged using light microscopy with micrographs displaying the struts of the collagen matrix and the

individual cells seeded around each of the struts (**Figure 1-6**). The cellular contractile forces were calculated by computing the critical force required to buckle a strut of known stiffness, length, and diameter using Euler's buckling relation.

Using this method, the group was able to determine how cellular contractile forces varied with the porosity of the matrix, the number of cells around a strut, and with the stiffness of the struts (64, 65). This method combines the benefits of 2D methods in that it uses fewer assumptions to calculate individual cellular contractile forces, while still creating a 3D environment that well matches *in vivo*. However, the major limitation in this method, as well as the others, is that it is only able to consider contractile forces exerted by cells on an ECM and is not able to measure the contractile forces cells exert on one another that are transmitted through cell-cell adhesions.

1.4. Reductionist Approaches to Quantify Protein Coupling

Although cell-cell adhesion is thought to have a major role in force transduction, missing is a method to measure these forces in a 3D environment. Using reductionist approaches, there has been much research on two major components of this force generation: actomyosin contraction and the binding of cadherin molecules.

1.4.1. Quantifying Actomyosin Coupling

Using reductionist approaches, a number of parameters regarding actomyosin coupling have been quantified. Parameters that have been measured include the force, displacement, and energy of hydrolysis involved in actomyosin contractility. To measure the force of a single myosin molecule reacting with an actin filament, an optical trap method was developed. In this method, an immobilized actin filament is brought into the vicinity of a single myosin molecule which is tethered to a fluorescently labeled bead that is attached to a glass coverslip (66). As the myosin head binds to the actin filament, there is a displacement of the fluorescent bead. This displacement is measured optically. Based on the displacement and stiffness of the bead, the force and the step of the myosin on the actin filament were quantified to be 3-4 pN and 11 nm, respectively. In addition, using modeling data of equilibrium constants, researchers also examined the energy involved in the hydrolysis of ATP by a single myosin II molecule and found the value to be 100×10^{-21} J (67).

1.4.2. Quantifying Cadherin Binding

In addition to examining the role of actomyosin coupling, researchers have also used reductionist approaches to determine the binding energy of another key molecule in cell-cell force generation, the cadherin. Sivasankar et al. measured the adhesive forces between bound cadherins by fabricating an artificial monolayer of cadherins. A second monolayer of cadherins, adhered to the tip of an AFM cantilever was introduced to the first, allowed to form adhesions and then pulled away. Using standard AFM measurement techniques, the energy of adhesion was measured to be 4 to 48 x 10^{-21} J (68).

Although these reductionist approaches have provided valuable information about the forces and energies of the proteins involved in cellular contractility, and planar and 3D substrates have provided very useful information about the contractile forces of cells reacting with an ECM, what is missing is a global systems biology approach method to look at cellular forces and energies in a 3D environment where cell-cell interactions dominate. Self-assembled microtissues are a scaffold free 3D platform in which cell-cell interactions dominate and thus may be useful for studying cellular forces.

1.5. Self-Assembled Microtissues (sections 1.5-1.5.1.1 contain excerpts from (69) published in 2010 in the *Wound Healing Society Yearbook*)

Self-assembly is the process by which mono-dispersed cells will aggregate via cell-to-cell adhesions; thus, forming a 3D cellular aggregate or microtissue. In self-assembled microtissues, the only ECM present is that which is produced by the cells. Microtissues exhibit properties closer to that of native tissues including microtissues of myocardial cells that beat with a human-like rhythm, hepatocyte microtissues that have superior detoxifying function, cartilage microtissues that maintain their differentiated phenotype, dorsal root ganglion cells extending projections into fibroblast microtissues, and human endothelial cells vascularizing fibroblast microtissues (70-73).

1.5.1. Methods of Self-Assembly

Traditionally there are many methods to form self-assembled microtissues including liquid overlay, spinner culture, and hanging drop; however, each have associated limitations. In liquid overlay, cells are seeded onto a flat non-adhesive material such as agarose and with small amounts of shaking, the cells aggregate and form spherical microtissues (spheroids). However, there is a large and heterogeneous distribution in the sizes of the spheroids and also a small yield of microtissues. The spinner culture and rotating wall vessel methods prevent cells from settling and as they collide with one another they form spheroids (74-76). Although these methods can form large numbers of microtissues, it is difficult to control size and so sizes vary. In the hanging drop method, a small volume of cell suspension is pippetted onto the surface of a Petri dish lid, which is

inverted causing the cells to settle to the bottom of the drop where they form spheroids. Spheroid size is less variable, but the method is labor intensive and it is difficult to change medium or harvest spheroids. None of these methods can self-assemble microtissues with complex shapes.

1.5.1.1. Directed Self-Assembly

Many of the limitations of the past methods were overcome when our lab developed a new method based on micro-molded non-adhesive hydrogels for the self-assembly of 3D microtissues (77, 78). This versatile technology starts with computer aided design software and uses rapid prototyping and replica molding to make a polydimethylsiloxane (PDMS) rubber mold for casting agarose gels. In one design, the PDMS mold has an array of 820 cylindrical pegs, which are 800 μm tall, each with a hemispherical cap. These pegs are situated on a rectangular stage. Molten agarose is added to the PDMS mold and after separation from the PDMS mold, the resulting agarose gel has a seeding chamber with 820 small recesses. The gels are equilibrated in cell culture medium and when a cell suspension is added to the seeding chamber, the cells settle to the bottom of the small recesses. Because the agarose environment is non-adhesive, the cells attach to one another and form a single spherical microtissue at the bottom of each recess. In a single pipetting step it is possible to form 820 microtissues. The hydrogel technology has the high throughput and ease of handling of the spinner culture method combined with the size consistency of the hanging drop method. The method has been used with a variety of cell types derived from many tissues including the skin, brain, liver, heart,

artery, breast, and ovary. To date, over 20 different cell types have been tested. Because the gels are transparent, the process of self-assembly can be monitored by microscopy.

In addition to forming large numbers of uniform sized microtissues in a single step, the micro-molded gels have several other practical advantages. First, microtissue size can be easily controlled by adjusting the number of cells seeded. Fewer cells form smaller microtissues. Second, microtissues with two or more cell types can be formed by seeding a mixture of cells. The ratio of cells in the microtissue is controlled by the ratio of cells in the mixture. Lastly, changing the medium or adding growth factors or even a second batch of cells is easy to do because the microtissues are at the bottom of the recesses.

A key advance uncovered with the micro-molded hydrogel technology, is the observation that self-assembly is not limited to spherical structures, cells can be directed to self-assemble complex shaped structures such as a honeycomb (77-79). Past methods were not able to form shapes other than spheroids. In fact, it was thought that cells could only self-assemble a spheroid, because that structure minimized surface free energy. Micro-molded hydrogels can also be used for the assembly of rod, toroid, loop-ended dogbone, and honeycomb shaped microtissues by changing the design of the recess features (77-79).

1.5.2. The Role of Adhesion and Contraction in Self-Assembly

Using complex shaped microtissues, such as the rod and the toroid, it was determined that cellular contraction plays a role in the self-assembly of microtissues. Previously, it was thought that self-assembly was a completely passive process (80). And that the only

factor that determined the self-assembly behavior of a microtissue was its apparent surface tension. And this surface tension was based solely on the expression of one protein, the cadherin (81). It was not until recently that the role of active cellular contraction was implicated in the self-assembly process. Using complex shaped microtissues, Dean et al. looked at the rate at which elongated rod shaped microtissues contracted towards a spherical microtissue (79). With this assay, the self-assembly kinetics of different cell types was determined. As well, using Y-27632, an inhibitor of ROCK mediated cellular contraction, it was also shown that the self-assembly kinetics of fibroblast microtissues was slowed significantly, indicating the importance of cellular contraction to the self-assembly process (82).

Using the toroid, Dean et al. further demonstrated the role of cellular contraction in the self-assembly of microtissues. It was shown that when cells are seeded in toroid recesses that the cells will settle in the circular trough of the hydrogel, self-assemble and then climb up the central cone of the hydrogel. Not only were these microtissues tightly wrapped around the central peg and under tension, but also the rate and degree of climbing up the peg was mediated by cellular contraction (82). With this research done by Dean et al. and by other groups, it was revealed that contraction is important in the self-assembly of microtissues making these tissues a good platform for studying the role of cellular contraction in an environment where cell-cell interactions dominate (79, 82-84).

However, what is missing with self-assembled microtissues is quantitative information about the forces and energies involved in the formation of these microtissues. Research done on planar substrates and 3D gels as well as experiments examining protein binding are quantitative in nature. So for self-assembled microtissues to be useful for studying cellular mechanics, they need to provide quantitative data for the forces and energies involved in cell-cell interactions.

1.6. Specific Aims

Specific Aim 1 **– To develop a systems biology approach to quantify the forces involved in the self-assembly of cells into microtissues**.

A number of assays have been developed to measure the forces and energies in protein coupling, the forces of cells on planar substrates, and the forces of cells interacting with a 3D gel or scaffold. However, each of these methods has associated limitations. Protein coupling only looks at a single component in the force generation system in isolation from other components. Planar substrates cause cells to take on a flat morphology and only consider the interactions of a single cell with an ECM. Collagen gels are only useful for understanding cellular forces exerted on an ECM. As well, many of these methods are only useful for cells that are known for their contractile properties. Needed is a systems biology approach to measure the forces and energies associated with a group of cells interacting with one another in a 3D environment.

A quantitative assay using self-assembled microtissues would be useful for examining cellular forces and energies in a 3D environment in which cell-cell interactions dominate. Self-assembled microtissues are scaffold free and thus maximize cell-cell interactions. Previously, using these microtissues, the kinetics of self-assembly was evaluated for a number of cell types with a number of tissue origins making it a useful platform for both contractile cells as well as cells not known for their contractile properties. As well, research has demonstrated the importance of cell mediated contraction as well as cell

adhesion in the self-assembly process making them ideal for looking at cellular forces and energies in an environment where cell-cell interactions dominate.

Specific Aim 2 **– To quantify the contribution of active cellular contraction to the self-assembly of cells into microtissues.**

The past 50 years of self-assembly research has focused on the role of passive surface interactions in the self-assembly of mono-dispersed cells into spherical microtissues (85). Researchers believed that the 3D conformation and sorting patterns of cells was determined solely by the apparent surface tension of a microtissue which in itself is solely determined by cadherin expression (75, 80, 81). However, recent work by Krieg et al. has brought to light that the cadherin may not be the only key player in the self-assembly and sorting patterns of cells by demonstrating the importance of actomyosin contractility (84). As well Dean et al. demonstrated that cytoskeletal mediated contraction contributes greatly to the self-assembly kinetics, stability, and self-sorting of rod, toroid, and dogbone shaped microtissues (79, 82, 83). Although these findings were quite pivotal to the field, and highlighted the importance of cellular contraction, they were mostly qualitative in nature.

Using 2D and 3D substrates the contribution of myosin II, actin polymerization, ROCK and MLCK mediated contraction have all been measured quantitatively. But once again, each of these methods only evaluates cell-ECM contraction. Measuring the forces and energies generated by cell-cell interactions would have great importance in a number of

fields, in which cell-cell interactions are important, including wound healing, fibrosis, morphogenesis, and metastasis.

***Specific Aim 3* – To quantify the forces involved in the self-assembly of microtissues that contain more than one cell type (mixed or heterotypic microtissues).**

Much of the research looking at cellular forces has only considered a single cell type in isolation; however, most tissues are made up of a number of cell types which contact and interact with one another. These heterotypic cell interactions are thought to be important for a number of physiological processes. Demonstrating the complexity of heterotypic interactions it has been shown on the molecular level that types of cadherin binding in itself is not responsible for self-sorting of cells and that all cadherins types have the same binding energy (86). Self-assembled microtissues have been used with a number of cell types to demonstrate the complexity of heterotypic cell interactions. Some example include, the increased albumin secretion when 3T3 fibroblasts are co-cultured with hepatocytes (87), the restoration of E-cadherin expression in prostate carcinoma cells when co-seeded with hepatocytes (88), the stabilization of NHF microtissues when seeded with H35s (79), and the successful self-assembly of keratinocytes into microtissues when seeded with dermal papilla cells (89). As well in 2D, heterotypic adhesion between an epitheliocyte and fibroblast has been shown to result in the fibroblast locally rearranging the cytoskeleton of the epitheliocyte within an hour after contact (90). These results demonstrate that heterotypic interactions result in complex cell

behavior. Despite the importance of heterotypic cell interactions, there is little quantitative understanding of the forces and energies involved in these interactions on the cell and tissue level.

1.7. References

1. Ethier CR & Simmons SA (2007) *Introductory Biomechanics: From Cells to Organisms* (Cambridge University Press, Cambridge).
2. Mammoto T & Ingber DE (2010) Mechanical control of tissue and organ development. *Development* 137(9):1407-1420.
3. Forouhar AS*, et al.* (2006) The embryonic vertebrate heart tube is a dynamic suction pump. *Science* 312(5774):751-753.
4. Hove JR*, et al.* (2003) Intracardiac fluid forces are an essential epigenetic factor for embryonic cardiogenesis. *Nature* 421(6919):172-177.
5. Ohashi N, Robling AG, Burr DB, & Turner CH (2002) The effects of dynamic axial loading on the rat growth plate. *J Bone Miner Res* 17(2):284-292.
6. Stokes IA, Mente PL, Iatridis JC, Farnum CE, & Aronsson DD (2002) Enlargement of growth plate chondrocytes modulated by sustained mechanical loading. *J Bone Joint Surg Am* 84A(10):1842-1848.
7. Cohen JC & Larson JE (2006) Cystic fibrosis transmembrane conductance regulator (CFTR) dependent cytoskeletal tension during lung organogenesis. *Dev Dynam* 235(10):2736-2748.
8. Moore KA*, et al.* (2005) Control of basement membrane remodeling and epithelial branching morphogenesis in embryonic lung by Rho and cytoskeletal tension. *Dev Dynam* 232(2):268-281.

9. Serluca FC, Drummond IA, & Fishman MC (2002) Endothelial signaling in kidney morphogenesis: A role for hemodynamic forces. *Current Biology* 12(6):492-497.

10. Moore SW, Biais N, & Sheetz MP (2009) Traction on Immobilized Netrin-1 Is Sufficient to Reorient Axons. *Science* 325(5937):166-166.

11. Lucitti JL*, et al.* (2007) Vascular remodeling of the mouse yolk sac requires hemodynamic force. *Development* 134(18):3317-3326.

12. Rodriguez-Boulan E, Paskiet KT, & Sabatini DD (1983) Assembly of enveloped viruses in Madin-Darby canine kidney cells: polarized budding from single attached cells and from clusters of cells in suspension. *J Cell Biol* 96(3):866-874.

13. Riethmacher D, Brinkmann V, & Birchmeier C (1995) A targeted mutation in the mouse E-cadherin gene results in defective preimplantation development. *Proc Natl Acad Sci U S A* 92(3):855-859.

14. Sawyer JM*, et al.* (2010) Apical constriction: a cell shape change that can drive morphogenesis. *Dev Biol* 341(1):5-19.

15. Ingber DE (2006) Mechanical control of tissue morphogenesis during embryological development. *Int J Dev Biol* 50(2-3):255-266.

16. Huang S & Ingber DE (1999) The structural and mechanical complexity of cell-growth control. *Nat Cell Biol* 1(5):E131-138.

17. Beloussov LV, Dorfman JG, & Cherdantzev VG (1975) Mechanical stresses and morphological patterns in amphibian embryos. *J Embryol Exp Morphol* 34(3):559-574.

18. Wallace K, Burt AD, & Wright MC (2008) Liver fibrosis. *Biochem J* 411(1):1-18.

19. Guarino M, Tosoni A, & Nebuloni M (2009) Direct contribution of epithelium to organ fibrosis: epithelial-mesenchymal transition. *Hum Pathol* 40(10):1365-1376.

20. Gabbiani G (2003) The myofibroblast in wound healing and fibrocontractive diseases. *J Pathol* 200(4):500-503.

21. Burridge K & Chrzanowska-Wodnicka M (1996) Focal adhesions, contractility, and signaling. *Annu Rev Cell Dev Biol* 12:463-518.

22. Dugina V, Fontao L, Chaponnier C, Vasiliev J, & Gabbiani G (2001) Focal adhesion features during myofibroblastic differentiation are controlled by intracellular and extracellular factors. *J Cell Sci* 114(Pt 18):3285-3296.

23. Grinnell F (1994) Fibroblasts, myofibroblasts, and wound contraction. *J Cell Biol* 124(4):401-404.

24. Burridge K (1981) Are stress fibres contractile? *Nature* 294(5843):691-692.

25. Discher DE, Janmey P, & Wang YL (2005) Tissue cells feel and respond to the stiffness of their substrate. *Science* 310(5751):1139-1143.

26. Halliday NL & Tomasek JJ (1995) Mechanical properties of the extracellular matrix influence fibronectin fibril assembly in vitro. *Exp Cell Res* 217(1):109-117.

27. Grinnell F (2000) Fibroblast-collagen-matrix contraction: growth-factor signalling and mechanical loading. *Trends Cell Biol* 10(9):362-365.

28. Harris AK, Wild P, & Stopak D (1980) Silicone rubber substrata: a new wrinkle in the study of cell locomotion. *Science* 208(4440):177-179.

29. Pelham RJ, Jr. & Wang YL (1998) Cell locomotion and focal adhesions are regulated by the mechanical properties of the substrate. *Biol Bull* 194(3):348-349; discussion 349-350.

30. Serini G*, et al.* (1998) The fibronectin domain ED-A is crucial for myofibroblastic phenotype induction by transforming growth factor-beta1. *J Cell Biol* 142(3):873-881.

31. Goldstein LS & Yang Z (2000) Microtubule-based transport systems in neurons: the roles of kinesins and dyneins. *Annu Rev Neurosci* 23:39-71.

32. Oshima RG (2007) Intermediate filaments: a historical perspective. *Exp Cell Res* 313(10):1981-1994.

33. Ananthakrishnan R & Ehrlicher A (2007) The forces behind cell movement. *Int J Biol Sci* 3(5):303-317.

34. Cooper GM & Hausman RE (2004) *The Cell: A Molecular Approach* (ASM Press, Washington, D.C.) Third Ed.

35. Katoh K, Kano Y, Amano M, Kaibuchi K, & Fujiwara K (2001) Stress fiber organization regulated by MLCK and Rho-kinase in cultured human fibroblasts. *Am J Physiol Cell Physiol* 280(6):C1669-1679.

36. Amano M*, et al.* (1998) Myosin II activation promotes neurite retraction during the action of Rho and Rho-kinase. *Genes Cells* 3(3):177-188.

37. Chen CS, Tan J, & Tien J (2004) Mechanotransduction at cell-matrix and cell-cell contacts. *Annu Rev Biomed Eng* 6:275-302.

38. Dunn GA & Brown AF (1986) Alignment of fibroblasts on grooved surfaces described by a simple geometric transformation. *J Cell Sci* 83:313-340.

39. Brunette DM & Chehroudi B (1999) The effects of the surface topography of micromachined titanium substrata on cell behavior in vitro and in vivo. *J Biomech Eng* 121(1):49-57.

40. Bissell MJ*, et al.* (1999) Tissue structure, nuclear organization, and gene expression in normal and malignant breast. *Cancer Res* 59(7 Suppl):1757-1763s; discussion 1763s-1764s.

41. Choquet D, Felsenfeld DP, & Sheetz MP (1997) Extracellular matrix rigidity causes strengthening of integrin-cytoskeleton linkages. *Cell* 88(1):39-48.

42. Wang N, Butler JP, & Ingber DE (1993) Mechanotransduction across the cell surface and through the cytoskeleton. *Science* 260(5111):1124-1127.

43. Riveline D*, et al.* (2001) Focal contacts as mechanosensors: externally applied local mechanical force induces growth of focal contacts by an mDia1-dependent and ROCK-independent mechanism. *J Cell Biol* 153(6):1175-1186.

44. Pelham RJ, Jr. & Wang Y (1997) Cell locomotion and focal adhesions are regulated by substrate flexibility. *Proc Natl Acad Sci U S A* 94(25):13661-13665.

45. Ko KS, Arora PD, & McCulloch CA (2001) Cadherins mediate intercellular mechanical signaling in fibroblasts by activation of stretch-sensitive calcium-permeable channels. *J Biol Chem* 276(38):35967-35977.

46. Ragsdale GK, Phelps J, & Luby-Phelps K (1997) Viscoelastic response of fibroblasts to tension transmitted through adherens junctions. *Biophys J* 73(5):2798-2808.

47. Hinz B & Gabbiani G (2003) Cell-matrix and cell-cell contacts of myofibroblasts: role in connective tissue remodeling. *Thromb Haemost* 90(6):993-1002.

48. Dembo M & Wang YL (1999) Stresses at the cell-to-substrate interface during locomotion of fibroblasts. *Biophys J* 76(4):2307-2316.

49. Pelham RJ, Jr. & Wang Y (1999) High resolution detection of mechanical forces exerted by locomoting fibroblasts on the substrate. *Mol Biol Cell* 10(4):935-945.

50. Choi CK, Breckenridge MT, & Chen CS (2010) Engineered materials and the cellular microenvironment: a strengthening interface between cell biology and bioengineering. *Trends Cell Biol* 20(12):705-714.

51. Roy P, Rajfur Z, Pomorski P, & Jacobson K (2002) Microscope-based techniques to study cell adhesion and migration. *Nat Cell Biol* 4(4):E91-96.

52. Tan JL*, et al.* (2003) Cells lying on a bed of microneedles: an approach to isolate mechanical force. *Proc Natl Acad Sci U S A* 100(4):1484-1489.

53. Jeon H, Kim E, & Grigoropoulos CP (2011) Measurement of contractile forces generated by individual fibroblasts on self-standing fiber scaffolds. *Biomed Microdevices* 13(1):107-115.

54. Bell E, Ivarsson B, & Merrill C (1979) Production of a tissue-like structure by contraction of collagen lattices by human fibroblasts of different proliferative potential in vitro. *Proc Natl Acad Sci U S A* 76(3):1274-1278.

55. Delvoye P, Wiliquet P, Leveque JL, Nusgens BV, & Lapiere CM (1991) Measurement of mechanical forces generated by skin fibroblasts embedded in a three-dimensional collagen gel. *J Invest Dermatol* 97(5):898-902.

56. Kolodney MS & Wysolmerski RB (1992) Isometric contraction by fibroblasts and endothelial cells in tissue culture: a quantitative study. *J Cell Biol* 117(1):73-82.

57. Freyman TM, Yannas IV, Yokoo R, & Gibson LJ (2001) Fibroblast contraction of a collagen-GAG matrix. *Biomaterials* 22(21):2883-2891.

58. Eastwood M, McGrouther DA, & Brown RA (1994) A culture force monitor for measurement of contraction forces generated in human dermal fibroblast cultures: evidence for cell-matrix mechanical signalling. *Biochim Biophys Acta* 1201(2):186-192.

59. Freyman TM, Yannas IV, Pek YS, Yokoo R, & Gibson LJ (2001) Micromechanics of fibroblast contraction of a collagen-GAG matrix. *Exp Cell Res* 269(1):140-153.

60. Freyman TM, Yannas IV, Yokoo R, & Gibson LJ (2002) Fibroblast contractile force is independent of the stiffness which resists the contraction. *Exp Cell Res* 272(2):153-162.

61. John J, Quinlan AT, Silvestri C, & Billiar K (2010) Boundary stiffness regulates fibroblast behavior in collagen gels. *Ann Biomed Eng* 38(3):658-673.

62. Legant WR*, et al.* (2009) Microfabricated tissue gauges to measure and manipulate forces from 3D microtissues. *Proc Natl Acad Sci U S A* 106(25):10097-10102.

63. Roy P, Petroll WM, Cavanagh HD, Chuong CJ, & Jester JV (1997) An in vitro force measurement assay to study the early mechanical interaction between corneal fibroblasts and collagen matrix. *Exp Cell Res* 232(1):106-117.

64. Harley BA, Freyman TM, Wong MQ, & Gibson LJ (2007) A new technique for calculating individual dermal fibroblast contractile forces generated within collagen-GAG scaffolds. *Biophys J* 93(8):2911-2922.

65. Corin KA & Gibson LJ (2010) Cell contraction forces in scaffolds with varying pore size and cell density. *Biomaterials* 31(18):4835-4845.

66. Finer JT, Simmons RM, & Spudich JA (1994) Single myosin molecule mechanics: piconewton forces and nanometre steps. *Nature* 368(6467):113-119.

67. Lan G & Sun SX (2005) Dynamics of myosin-driven skeletal muscle contraction: I. Steady-state force generation. *Biophys J* 88(6):4107-4117.

68. Sivasankar S, Gumbiner B, & Leckband D (2001) Direct measurements of multiple adhesive alignments and unbinding trajectories between cadherin extracellular domains. *Biophys J* 80(4):1758-1768.

69. Youssef J & Morgan JR (2010) Self-Assembled Scaffold-Free Three-Dimensional Microtissues for Tissue Repair. *Wound Healing Society Yearbook* 1:451-456.

70. Fukuda J & Nakazawa K (2005) Orderly arrangement of hepatocyte spheroids on a microfabricated chip. *Tissue Eng* 11(7-8):1254-1262.

71. Kelm JM & Fussenegger M (2004) Microscale tissue engineering using gravity-enforced cell assembly. *Trends Biotechnol* 22(4):195-202.

72. Kelm JM, Ittner LM, Born W, Djonov V, & Fussenegger M (2006) Self-assembly of sensory neurons into ganglia-like microtissues. *J Biotechnol* 121(1):86-101.

73. Kunz-Schughart LA*, et al.* (2006) Potential of fibroblasts to regulate the formation of three-dimensional vessel-like structures from endothelial cells in vitro. *Am J Physiol Cell Physiol* 290(5):C1385-1398.

74. Castaneda F & Kinne RK (2000) Short exposure to millimolar concentrations of ethanol induces apoptotic cell death in multicellular HepG2 spheroids. *J Cancer Res Clin Oncol* 126(6):305-310.

75. Foty RA & Steinberg MS (2005) The differential adhesion hypothesis: a direct evaluation. *Dev Biol* 278(1):255-263.

76. Manley P & Lelkes PI (2006) A novel real-time system to monitor cell aggregation and trajectories in rotating wall vessel bioreactors. *J Biotechnol* 125(3):416-424.

77. Napolitano AP, Chai P, Dean DM, & Morgan JR (2007) Dynamics of the self-assembly of complex cellular aggregates on micromolded nonadhesive hydrogels. *Tissue Eng* 13(8):2087-2094.

78. Napolitano AP*, et al.* (2007) Scaffold-free three-dimensional cell culture utilizing micromolded nonadhesive hydrogels. *Biotechniques* 43(4):494, 496-500.

79. Dean DM, Napolitano AP, Youssef J, & Morgan JR (2007) Rods, tori, and honeycombs: the directed self-assembly of microtissues with prescribed microscale geometries. *Faseb J* 21(14):4005-4012.

80. Foty RA, Pfleger CM, Forgacs G, & Steinberg MS (1996) Surface tensions of embryonic tissues predict their mutual envelopment behavior. *Development* 122(5):1611-1620.

81. Foty RA & Steinberg MS (2004) Cadherin-mediated cell-cell adhesion and tissue segregation in relation to malignancy. *Int J Dev Biol* 48(5-6):397-409.

82. Dean DM & Morgan JR (2008) Cytoskeletal-mediated tension modulates the directed self-assembly of microtissues. *Tissue Eng Part A* 14(12):1989-1997.

83. Dean DM, Rago AP, & Morgan JR (2009) Fibroblast elongation and dendritic extensions in constrained versus unconstrained microtissues. *Cell Motil Cytoskeleton* 66(3):129-141.

84. Krieg M*, et al.* (2008) Tensile forces govern germ-layer organization in zebrafish. *Nat Cell Biol* 10(4):429-436.

85. Steinberg MS (1962) Mechanism of tissue reconstruction by dissociated cells. II. Time-course of events. *Science* 137:762-763.

86. Shi Q, Chien YH, & Leckband D (2008) Biophysical properties of cadherin bonds do not predict cell sorting. *J Biol Chem* 283(42):28454-28463.

87. Luo Y, Kobler JB, Zeitels SM, & Langer R (2006) Effects of Growth Factors on Extracellular Matrix Production by Vocal Fold Fibroblasts in 3-Dimensional Culture. *Tissue Eng*.

88. Yates CC, Shepard CR, Stolz DB, & Wells A (2007) Co-culturing human prostate carcinoma cells with hepatocytes leads to increased expression of E-cadherin. *Br J Cancer* 96(8):1246-1252.

89. Yen CM, Chan CC, & Lin SJ (2010) High-throughput reconstitution of epithelial-mesenchymal interaction in folliculoid microtissues by biomaterial-facilitated self-assembly of dissociated heterotypic adult cells. *Biomaterials* 31(15):4341-4352.

90. Omelchenko T*, et al.* (2001) Contact interactions between epitheliocytes and fibroblasts: formation of heterotypic cadherin-containing adhesion sites is accompanied by local cytoskeletal reorganization. *Proc Natl Acad Sci U S A* 98(15):8632-8637.

1.8. Figures

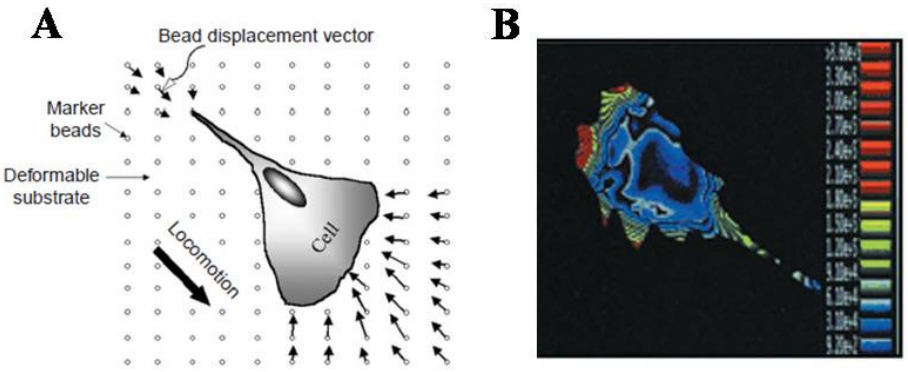

Figure 1-1: Traction force microscopy can identify the magnitude, direction, and location of forces generated by cells. (A) Schematic of traction force microscopy used to measure cellular forces. As cells attach to the polyacrylamide gel, they spread, and exert traction forces. The forces involved in traction and locomotion result in a displacement of the marker beads within the gel. (B) Representative image of forces generated by a cell during locomotion (51).

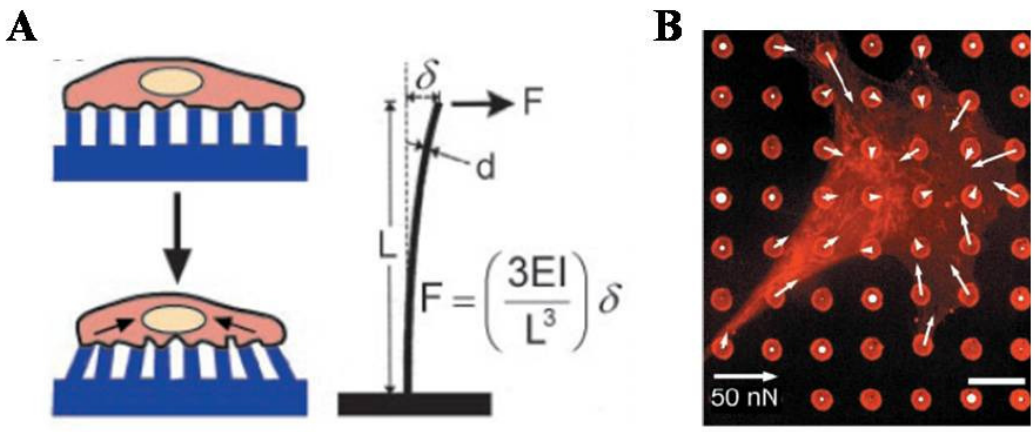

Figure 1-2: mPADs use beam theory to measure the contractile forces of cells. (A) Schematic of cells seeded on mPADs. As cells attach to the microneedles they exert traction forces which result in the deflection of the beams. The force of contraction on each beam is measured as $F=(3EI/L^3)\delta$, where E is the elastic modulus of PDMS, I is the moment of inertia for a beam, L is the length of the beam, and δ is the deflection of the beam. (B) Representative image of the force vectors of contracting cells on mPADs.

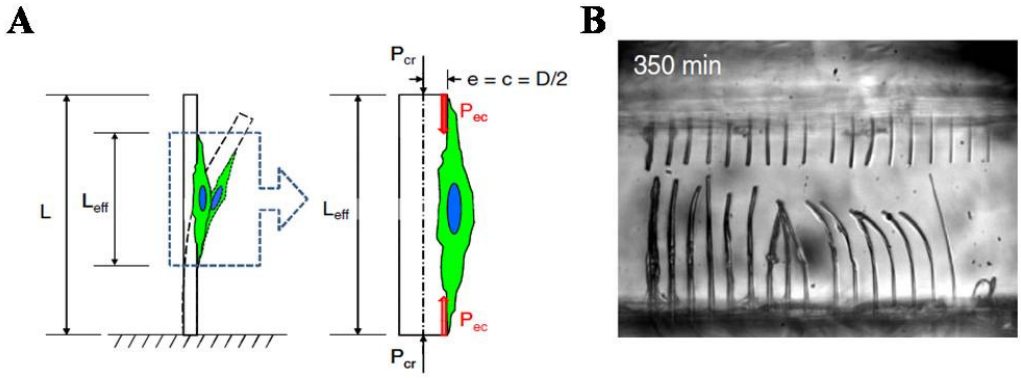

Figure 1-3: Cells on self standing scaffolds are used to measure the forces exerted by cells on a fiber. (A) Schematic of cells seeded on self-standing scaffolds. As the cells settle and attach to the fibers, they exert contractile forces which are calculated from the length of contact of the cell, the length of the fiber, the stiffness of the fiber, its moment of inertia, and its deflection. (B) Micrograph of cells seeded on self-standing scaffolds after 350 minutes. Adapted from (53)

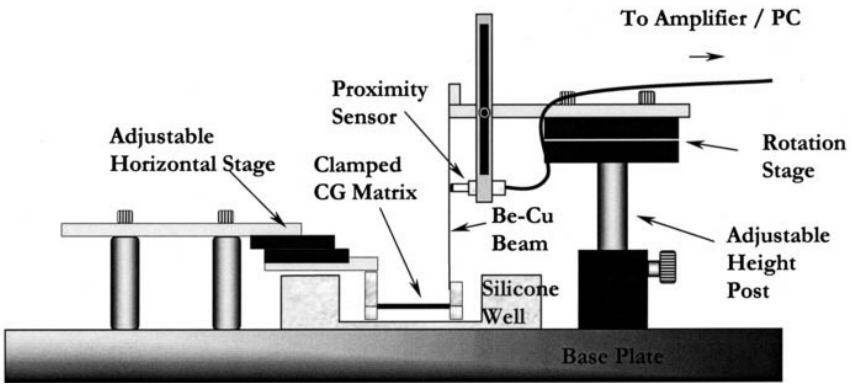

Figure 1-4: Schematic of the culture force monitor used to measure cellular contractile forces in collagen matrices (60).

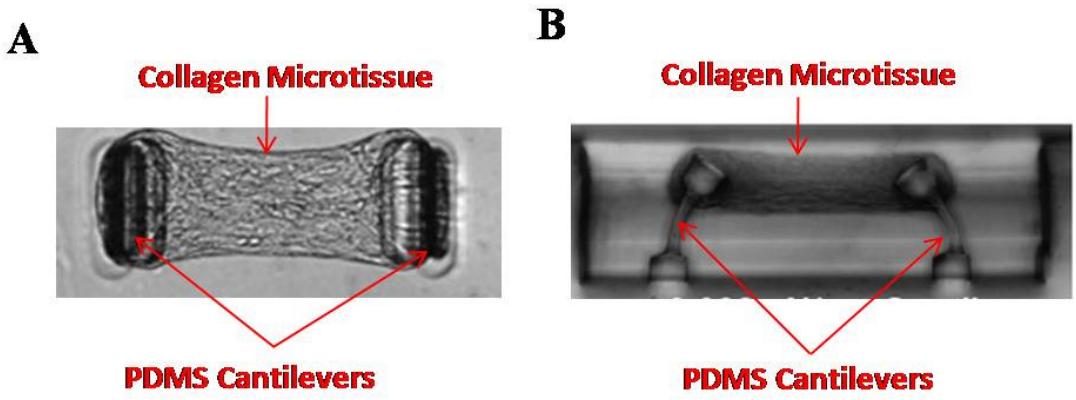

Figure 1-5: Top (A) and side view (B) images of μTUGs used to measure contractile forces of cells within microscale collagen gels. Images modified from (62).

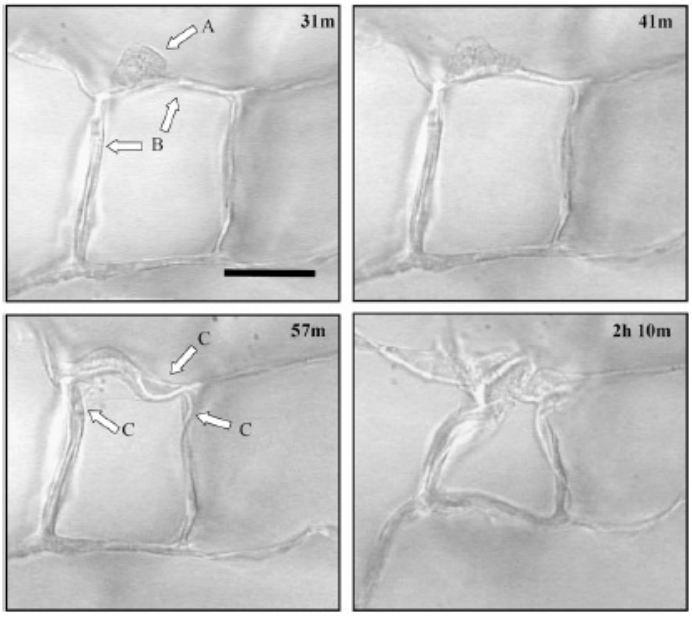

Figure 1-6: Fibroblasts buckle the struts of collagen matrices. (A) 31 minutes post seeding a rounded fibroblast settles around the struts (B) of the matrix. After 41 minutes the cells have spread along the strut. At 57 minutes there are many locations (C) in which the struts have begun to bend. After 2 hours and 10 minutes, the struts are buckled by the cell (64).

CHAPTER 2

2. Quantification of the Forces Driving Self-Assembly of 3D Microtissues

Jacquelyn Youssef, Asha Nurse, Lambert B. Freund, and Jeffrey R. Morgan

The following chapter was published in PNAS online before print April 11, 2011, doi: 10.1073/pnas.1102559108

2.1.Abstract

In a non-adhesive environment, cells will self-assemble into microtissues, a process relevant to tissue engineering. Although this has been recognized for some time, there is no basis for quantitative characterization of this complex process. Here we describe a recently developed assay designed to quantify aspects of the process and discuss its application in comparing behaviors between cell types. Cells were seeded into nonadhesive micromolded wells, each well with a circular trough at its base formed by the cylindrical sidewalls and by a central peg in the form of a right circular cone. Cells

settled into the trough and coalesced into a toroid, which was then driven up the conical peg by the forces of self-assembly. The mass of the toroid and its rate of upward movement were used to calculate the cell power expended in the process against gravity. The power of the toroid was found to be 0.31±0.01 pJ/h and 4.3±1.7 pJ/h for hepatocyte cells and fibroblasts, respectively. Blocking Rho kinase by means of Y-27632, resulted in a 50% and greater reduction in power expended by each type of toroid, indicating that cytoskeletal-mediated contraction plays a significant role in the self-assembly of both cell types. Whereas the driving force for self-assembly has often been viewed as the binding of surface proteins, these data show that cellular contraction is important for cell-to-cell adhesion. The power measurement quantifies the contribution of cell contraction and will be useful for understanding the concerted action of the mechanisms that drive self-assembly.

2.2. Introduction

The self-assembly of cells into microtissues, often viewed as a passive process driven by chemical forces resulting from binding of cadherins expressed on cell surfaces (1, 2), is now thought to be a more complex process. Recent work has shown that the cytoskeleton also plays an important role in force generation, stability and self-sorting of microtissues (3-6). Thus, self-assembly is a complex process involving multiple protein mechanisms working in concert.

Self-assembly and the cell-to-cell adhesion that drives it are relevant to tissue formation, morphogenesis and disease. However, little quantitative data are available on the forces driving self-assembly. At the molecular level, precise measurements of the binding strength and energy of adhesion of surface proteins (7, 8) as well as the force of contraction of the actin cytoskeleton (9, 10) have been made. On the cellular level, traction force microscopy has been used to measure the adhesion forces of single cells on flat substrates (11-13), and fibroblast populated collagen gels have been used in the study of cell-matrix interactions (14). However, cell-to-cell interactions in a three-dimensional (3D) environment have not been fully investigated. Doing so requires a quantitative systems biology approach that can be used not only to quantify the aggregation and self-assembly of groups of cells, but also to quantify the contributions of specific proteins and protein systems to the process.

In the past, we have reported, observations on the behavior of mono-dispersed normal human fibroblasts (NHFs) when seeded in a non-adhesive micro-molded hydrogel cylindrical well (15). For the case of a well with a base in the form of a circular trough defined by the outer surface and a central conical peg, the cells rapidly self-assembled into a microtissue in the form of a multi-cellular toroid. The forces of self-assembly were strong enough to drive the toroid up the slope of the peg from its base to its summit (4). Here, we describe a novel assay to measure these forces. In particular, the assay provides a measure of cell power defined as the rate of work done against gravity as such a self-assembled multi-cellular toroid moves up a conical peg of known geometry. The assay was used to compare behaviors of two cell types, the NHF and a rat hepatocyte cell line (H35). We found that, regardless of the slope of the conical peg, rapidly self-assembling NHF toroidal microtissues reached a particular height in just two hours, whereas the H35 toroids assembled more slowly and required at least 48 hours to reach the same prescribed height for all slopes considered. These data were used to calculate the power of NHF toroids which was found to be an order of magnitude greater than that of the H35 toroids.

In addition to these comparisons, the contributions to the cell power of specific protein systems were quantified. When treated with the Rho kinase (ROCK) inhibitor Y-27632, power output of an NHF toroid decreased by approximately 50%. When H35 toroids were treated with the same inhibitor, their power output decreased by 85%, an unexpected result as H35s are not considered to be a contractile cell type. These data

indicate that active cellular contraction has an important role in the self-assembly of both highly contractile NHFs as well as the non-contractile H35s. The assay has the advantage of being a straightforward noninvasive, noncontact method for measuring the forces of self-assembly. Cell power is a quantitative systems biology measurement for comparing the behavior of different cell types with the potential to quantify the contributions of specific proteins or protein systems to the complex process of self-assembly.

2.3. Results

To investigate the forces governing the self-assembly of 3D microtissues from mono-dispersed cells, we chose the toroid and designed a 3D micro-mold made of polyacrylamide (**Figure 2-1**). This non-adhesive micro-mold contained a single row of toroid wells. To vary loading conditions, we fabricated micro-molds with conical pegs of differing slopes which were measured to be 84.2 $\pm$ 2.6º (85º), 65.9$\pm$ 4.9º (65º), and 55.1 $\pm$ 3.4º (55º). When a cell suspension was seeded, the cells settled to the bottom of the circular trough and were confined by the chamber wall at the outer edge of the trough and by a conical peg on the inner edge of the trough. As a result of cell-to-cell interactions, they assembled into toroidal microtissues. The integrity and symmetry of the toroid was maintained with the forces of self-assembly tending to drive the toroid up the cone (**Figure 2-2**)(**Supplemental Data, viewable online at www.pnas.org/lookup/suppl/doi:10.1073/pnas.1102559108/-/DCSupplemental.**).

To determine the minimum number of cells needed to form a toroid, we seeded micro-molds with varying numbers of either NHFs or H35s and assessed toroid formation after 17 hours for three slopes (**Figure 2-3**). For both cell types, toroid formation was 100% for all three slopes when seeded with 21,000 cells/toroid or greater. The cell number at which toroid formation was 50% for NHFs was 8,000, 6,000, and 5,000 cells for the 85º, 65º, and 55º slopes, respectively; and for the H35s it was 3,000 cells for all three slopes. These data suggest that the initial and rapid events of NHF toroid formation are slope (load) sensitive, but once formed, the NHF toroid is stable and progresses rapidly. For

subsequent experiments, we seeded micro-molds with 21,000 cells per well for both cell types to assure 100% toroid formation and to minimize size.

Using side view microscopy, we measured the vertical distance travelled by the toroid (height), its major radius, and its minor radius as it moved up the three slopes. Over an eight hour period, the height of NHF toroids increased with time and was comparable for all three slopes (**Figure 2-4**). In contrast, H35 toroids climbed the conical pegs at a much slower rate. Within two hours, NHF toroids moved an average of almost 170 μm for all three slopes. Whereas, H35 toroids were much slower and required 48, 72, and 96 hours on the 55º, 65º, and 85º slopes, respectively, to reach the height NHF toroids had attained in only 2 hours. Unlike the NHFs, the distance travelled by the H35 toroids was dependent on the slope of the peg with samples on the 65º and 85º slopes climbing an average of 33 and 50 μm less, respectively, in the first 24 hours, than the 55º samples. By changing the slope of the peg from 55º to 65º, the component of the toroid's weight opposing its motion is increased by 10%. Likewise, the change from 55º to 85º results in an 18% increase in loading. For H35 toroids, a 10% increase in loading (55º to 65º) decreased the height 28%, while an 18% increase in loading (55º to 85º) led to a 42% decrease in toroid height.

The values for the major and minor radii were used to calculate the volume of each toroid for the duration of the experiments using the equation: $V = 2\pi^2 ab^2$, where a is the major radius and b is the minor radius. Changes to the volume of the toroid for all three slopes

were not statistically significant, with volume fluctuations being less than 4.4%, 1.6%, and 1.6% for the 85º, 65º, and 55º slopes, respectively for the NHF microtissues and less than 0.5%, 3.6%, and 4.7% for the 85º, 65º, and 55º slopes, respectively for the H35 microtissues.

The cellular forces of self-assembly that drive the toroid up the cone must overcome the gravitational forces resisting its movement. To estimate the mass of the toroid, we measured the density of individual cells in cell culture medium and computed density from the settling rate. The density of single NHF and H35 cells was 1.05 $\pm$ 0.01 and 1.08 $\pm$ 0.02 g/cm^3, respectively. Thus, based on toroid volume and density of the cells, we calculated that a toroid of 21,000 NHFs has a mass of 4.36 μg and a toroid of the same number of H35s has a mass of 6.98 μg.

The rate at which the cellular forces of self-assembly work to move a toroid up the cone is power: $P=\Delta W/\Delta t$, where ΔW is work necessary to move a toroid of a given mass to a given height and Δt is the time over which the work is performed. Cell power is an indication of the rate of self-assembly in terms of the energy output. From measurements of toroid height and weight, we calculated cell power as a function of time (**Figure 2-5**). For both cell types, cell power gradually decreased over the course of the experiments; however, only the cell power of H35 toroids was dependent on slope. Specifically, at 2 hours, the power output of an NHF toroid was 3.8 $\pm$ 0.9 pJ/hour, 4.1 $\pm$ 1.6 pJ/hour, and 4.7 $\pm$ 1.6 pJ/hour for the 85º, 65º, and 55º slopes, respectively. Whereas, the power

exerted by an H35 toroid of same cell number to a height comparable to that of an NHF toroid, was only 0.24 ± 0.01 pJ/hour, 0.31 ± 0.01 pJ/hour, and 0.49± 0.04 pJ/hour for the 85º, 65º, and 55º slopes, respectively. If we assume that all cells within a microtissue exert equal power, the power per cell for all three slopes averaged to be 0.2 fJ/hour per NHF, and 0.02 fJ/hour per H35. For an H35 toroid to reach the height of NHF toroid in the same time, it would have to increase its power output by about 93%.

To elucidate the contribution of cytoskeletal mediated contraction, in terms of cell power, NHFs and H35s were treated with 10 and 100 μM of Y-27632, an inhibitor which blocks ROCK mediated contraction by preventing the formation of stress fibers and the phosphorylation of myosin light chains (MLC). Treated cells were seeded in micro-molds equilibrated in Y-27632 and side view images were taken at two hour intervals for eight hours for NHFs and at 24 hour intervals for 96 hours for H35s. Y-27632 treated toroids still moved up the conical pegs; but did not climb up as high as the untreated controls for both NHFs and H35s (**Figure 2-6**). Specifically, significant differences were seen between controls and treated samples (10 μM, and 100 μM Y-27632) for all three slopes. Toroid height and weight were used to analyze the power output of the NHFs (**Table 2-1**). After 2 hours, inhibiting ROCK (with both 10 and 100 μM Y-27632) led to a 49 ± 9% decrease in power for NHFs. Similar to NHFs, H35 treated toroids did not climb up as high as control samples with ROCK inhibition decreasing H35 toroid height for all three slopes in a dose dependent manner. Toroid sensitivity to slope was also exhibited with 65º and 85º drug treated samples stalling completely at later time points while the 55º

drug treated samples continued up the cone for the duration of the experiment. ROCK inhibition also substantially decreased H35 power output with an average power decrease of 58 $\pm$ 7% for the 10 μM and 83 $\pm$ 2% and for the 100 μM Y-27632 treated samples over all time points.

2.4. Discussion

Most studies on the cell-to-cell adhesion that drives self-assembly are qualitative and have focused on the self-sorting of a mixture of cells (1, 16), the role of cadherins (17), and the influence of surface tension (1, 2). In this study, we have developed a novel assay to measure cell power, a quantitative measure of the work output of self-assembling cells. The assay is well suited to measuring the small forces of self-assembly that occur with relatively slow kinetics in groups of living cells. Unlike other assays, which use compression testing (16), the assay does not contact or manipulate the microtissues which could alter its properties. Because the assay incorporates only time and the influence of gravity, loads on the microtissues are precise and reproducible and instrument calibrations are unnecessary. The geometry of the cone can be carefully controlled, reproduced and measured. Moreover, the influence of gravity can be modulated by changing the slope of the cone to induce a variety of loading conditions.

A power measurement is a systems quantitative measure of a multi-component system (mechanical, chemical, and surface energy) that drives self-assembly. Much attention has been focused on the role of cadherins and it has been shown that within a single cell type, expression of cadherins have a strong influence on self-assembly (2). But it has also been shown that cytoskeletal mediated tension affects self-assembly (3, 6). Further, it is well known that in addition to cadherins, cells have numerous other surface proteins responsible for cell-to-cell adhesion and that the types of these proteins and their levels vary widely between different cell types as do the proteins that participate in cytoskeletal

mediated tension (18-22). A power measurement takes into account the action of all these protein systems as well as those that might act to resist cell-to-cell adhesion such as differences in the stiffness and viscoelasticity of cells or levels of anti-adhesive proteins. Power measurements can be used as a point of reference for comparing cell types. We have observed that the driving forces behind the self-assembly of NHFs are significantly greater than H35s and are of a magnitude (strength and/or rate) that is unaffected (or unobservable) even under an 18% increase in loading.

Power measurements can also be used to quantify the specific contribution of cellular components to self-assembly. Recent work from our lab demonstrated that myosin motors participate in the stability (3, 5) and sorting (3) of NHF microtissues and others have shown their role in zebrafish embryos (6). When ROCK was inhibited in our experiments, power output of an NHF toroid decreased by about 50%. This result is not surprising for NHFs, a cell with well known contractile properties; but, when ROCK was inhibited in H35 toroids, power output decreased by 85% indicating the importance of the cytoskeleton in the self-assembly of both contractile and non-contractile cells. Although the power associated with ROCK in H35s is significantly lower than that of NHFs (0.25 compared to 2.1 pJ/hour, respectively), ROCK associated power is a larger proportion of the total power driving self-assembly of H35s compared to NHFs (85% versus 50%, respectively). Several reasons could explain why ROCK contributes a larger percentage to H35 self-assembly. H35s are a denser cell (0.03 g/cm^3 greater than NHF) and so when cellular contraction is blocked, the effect of the cell's weight could be further amplified.

When loading was decreased by lowering the slope of the peg, H35 toroids travelled further up the peg indicating that the weight of the microtissue is a limiting factor in its power output. Another possible explanation could be that NHFs have a radially arranged cytoskeletal network (3), while H35s, as an epithelial cell, have a cortically arranged cytoskeleton network (23). A radial cytoskeleton network may be more efficient at exerting power than a cortical cytoskeleton and so an even higher dose of Y-27632 may be necessary to fully block contraction in NHFs. A third reason may have to do with the pathways used for contraction. The ROCK system and the myosin regulatory light chain kinase system (MLCK) are two distinct pathways involved in contraction of NHFs (24, 25). By blocking the ROCK pathway in NHFs, the MLCK pathway may compensate and mask the full effect of blocking contraction. As well the MLCK pathway may not play as much of a role in the self-assembly of H35s as it does in NHFs. It is also possible that a greater proportion of NHF's self-assembly power reside with its surface binding proteins due to either higher expression and/or energy of these proteins.

One theory of self-assembly is that cells minimize surface free energy by maximizing intercellular adhesion (1). This theory also states that a mix of two different cell types will self-sort due to differences in adhesion and cohesion, like the behavior of two immiscible fluids (1). In this theory, the apparent surface tension is regarded as the sole factor determining the formation and structure of self-assembled microtissues. Within a single cell line it was demonstrated that spheroid surface tension was directly proportional to cadherin expression with cells with increased cadherin levels moving to

the center of mixed spheroids (2, 16, 17). With this model, the process of self-assembly was deemed to be passive and even likened to soap bubble formations (26). But recent data have shown that the strength or specificity of cadherin bonds alone do not predict sorting behavior in self-assembly (7). Our power measurements reveal that self-assembly is not a passive process and that cytoskeletal mediated tension is a major contributor for both cell types. As well, because cell power takes a systems biology approach, it may be useful for predicting the sorting behavior of different cell types as well as the sorting behavior of one cell type when a population of the cells has been treated to decrease or increase the function of a specific protein.

Power measurements may be an interesting point of reference between measurements of the energies of purified proteins as well as protein systems from single cells. The power output by an NHF toroid is 2.5 pJ (between 2 to 4 hrs, 65º slope) and the energy of cadherin bonding is 4 to 48 x 10^{-21} J/ cadherin bond (27). This power output is equivalent to the formation of 52 to 625 million cadherin bonds. If cadherin bonding alone drove the 20,000 μm^2 change in toroid surface area that occurs over 2 hours, we estimate it would require 2.6 to 31 thousand cadherins/μm^2 on the outer surface of the toroid (3 to 39 million cadherins per cell). When overexpressed by genetic modification there are 20,000 to 250,000 cadherins per cell and in cadherin binding strength experiments (8), artificial mono-layers have between 2,000 and 4,000 cadherins/μm^2 (27). Likewise, the forces produced by focal adhesions of single cells is ~30 nN in a period of 5 minutes (10). A cell with ~25 focal adhesions would have a power output of ~4 fJ/hour per cell, higher

than our measure of 0.2 fJ/hour per cell. Although it should be kept in mind that the focal adhesion measurements were made on a stiff substrate (megapascals) (10), and self-assembling microtissues are significantly less stiff (kilopascals) (11).

Lastly, unlike other models of self-assembly, a cell power analysis does not assume that the system is thermodynamically closed, nor is it confined by assumptions about how the system operates. For example, cell power does not assume that the system is driven solely by passive surface interactions, (which ignores proteins inside the cell and the chemical energy derived from ATP) nor does cell power assume that the system is driven by the cytoskeleton alone, ignoring the binding of surface proteins. A cell power measurement quantifies the amount of energy expended and so is a useful point of comparison for cell types from different tissues. And, as our ROCK inhibition data shows it can be used to quantify the contribution of specific proteins and protein systems to self- assembly regardless of their cellular location or mechanism of action. Such information is important to a fundamental understanding of cell-to-cell adhesion and may be useful for applications in tissue engineering. For example, cell power measurements could be used with selected pharmacologies or genetic tools to tailor the tissue assembly process. Previously, we have shown that H35s will readily form a stable microtissue in the shape of honeycombs or a loop ended dogbone; however, NHF microtissues in the same configuration will self-assemble, stretch and ultimately fail (4, 5). NHF dogbone structures can be stabilized by treatment with Y-27632 (5). From this study, we know that drug treated NHFs have a reduced power of 0.10 ± 0.01 fJ/hr per NHF and so power

measurements may be useful for predicting the stability of complex shaped microtissues. Power measurements may also be useful for understanding the self-sorting of mixtures of cells with those cells of higher cell power occupying the core of a spheroid. In a prior study, NHFs treated with Y-27632 formed the outer coating when mixed with untreated NHFs, and in mixes of NHFs and H35s, NHFs formed the inner core (3).

2.5. Methods and Materials

Micro-mold design and gel casting

Toroid molds were designed using the computer aided design (CAD) software Solid Works (Solid Works Corporation, Concord, MA). Three mold geometries were designed in which the slope of the central peg was modified to be 85º, 65º, and 55º. The circular round bottom troughs were 400 μm, 350 μm, to 300 μm in diameter and the central pegs were 600 μm, 650 μm, and 780 μm for the 85º, 65º, and 55º, respectively. For the 85º and 65º slopes the micro-molds contained twelve wells and for the 55º slope eleven wells. CAD files were used to produce thermowax molds with a rapid prototyping machine (3D Systems Corporation, Valencia, CA).

The wax molds were used to cast 13% polyacrylamide gels. Gels were removed from wax molds and transferred to six well culture plates. The gels were rinsed with fresh culture medium and then equilibrated overnight at 37ºC in 4 ml of DMEM supplemented with 10% fetal bovine serum (FBS) and 1% penicillin/streptomycin (pen/strep). After equilibration, the medium was removed, and the gels were rinsed with fresh medium.

Cell culture and gel seeding

NHFs (passage 3-10), derived from neonatal foreskins, and H35s (passage 4-12) were grown in T-175 flasks in DMEM with 10% FBS and 1% pen/strep at 37ºC and 10% CO_2. Cells were removed from flasks using a standard trypsin process. Briefly, cells were exposed to 0.05% trypsin for 10 minutes, quenched with serum containing medium, spun

down at 800 rpm for 6 minutes, resuspended in a known volume of medium, and counted. 70 µl of cell solution was added to each hydrogel. After 30 minutes, 3 ml of fresh medium was added to each of the wells. Images of the samples were taken every 2 hours for 8 hours for NHFs and every 24 hours for 96 hours for H35s. To determine the minimum number of cells necessary to form a stable toroid, 1,000 to 30,000 cells per well were seeded into the 85º, 65º, and 55º gels. Toroid formation was assessed using side view microscopy 17 hours after seeding.

For drug inhibition studies, Y-27632 (Sigma Aldrich, St. Louis, MO), was dissolved in culture medium and brought to a stock concentration of 200 µM. The stock solution was further diluted in culture medium to obtain solutions with concentrations of 10 and 100 µM. Prior to cell seeding, gels were equilibrated for at least 2 hours in drug containing medium and cells were resuspended in drug containing medium. Cells were then seeded into the gels and imaged.

Cell density measurements

Mono-dispersed cells were pippetted into the micro-molds and side view time lapse images were taken to measure the rate at which individual cells settled. Settling rates were used to calculate the density of the H35s and NHFs using a force balance for the drag force on a sphere moving at a constant speed through a viscous fluid. In the present instance, this balance is written in the form: $\rho_{cell} = \rho_{media} + \frac{6\pi\mu vr}{gV}$, where ρ_{cell} is the

density of a cell, ρ_{medium} is the density of the medium, μ is the dynamic viscosity of the medium, v is the rate at which the cell settles, r is the radius of the cell, and V is the volume of the cell.

Thus, based on the volume of the toroid and density of individual cells, we calculated that a toroid of 21,000 NHFs has a mass of 4.36 μg and a toroid of the same number of H35s has a mass of 6.98 μg.

Microscopy

To capture side view images a Mitutoyo FS-110 microscope was modified to lie on its back and a translational stage was added to hold samples. Samples were imaged in bright field through the eyepiece of the microscope. ImageJ Software (Rasband, W.S., ImageJ, NIH) was used measure the height of the toroid, the major radius, and the minor radius of the toroid, and the slope of the conical pegs.

2.6. Acknowledgments

This work was funded, in part by the MRSEC Program of the National Science Foundation under award DMR-0520651, the NIRT Program under award DMI-0506661 and NIH R01EB008664-01A1.

2.7. References

1. Steinberg MS (1962) Mechanism of tissue reconstruction by dissociated cells. II. Time-course of events. *Science* 137:762-763.
2. Foty RA & Steinberg MS (2005) The differential adhesion hypothesis: a direct evaluation. *Dev Biol* 278(1):255-263.
3. Dean DM & Morgan JR (2008) Cytoskeletal-mediated tension modulates the directed self-assembly of microtissues. *Tissue Eng Part A* 14(12):1989-1997.
4. Dean DM, Napolitano AP, Youssef J, & Morgan JR (2007) Rods, tori, and honeycombs: the directed self-assembly of microtissues with prescribed microscale geometries. *Faseb J* 21(14):4005-4012.
5. Dean DM, Rago AP, & Morgan JR (2009) Fibroblast elongation and dendritic extensions in constrained versus unconstrained microtissues. *Cell Motil Cytoskeleton* 66(3):129-141.
6. Krieg M*, et al.* (2008) Tensile forces govern germ-layer organization in zebrafish. *Nat Cell Biol* 10(4):429-436.

7. Shi Q, Chien YH, & Leckband D (2008) Biophysical properties of cadherin bonds do not predict cell sorting. *J Biol Chem* 283(42):28454-28463.

8. Sivasankar S, Gumbiner B, & Leckband D (2001) Direct measurements of multiple adhesive alignments and unbinding trajectories between cadherin extracellular domains. *Biophys J* 80(4):1758-1768.

9. Lan G & Sun SX (2005) Dynamics of myosin-driven skeletal muscle contraction: I. Steady-state force generation. *Biophys J* 88(6):4107-4117.

10. Tan JL*, et al.* (2003) Cells lying on a bed of microneedles: an approach to isolate mechanical force. *Proc Natl Acad Sci U S A* 100(4):1484-1489.

11. Discher DE, Janmey P, & Wang YL (2005) Tissue cells feel and respond to the stiffness of their substrate. *Science* 310(5751):1139-1143.

12. Harris AK, Wild P, & Stopak D (1980) Silicone rubber substrata: a new wrinkle in the study of cell locomotion. *Science* 208(4440):177-179.

13. Dembo M & Wang YL (1999) Stresses at the cell-to-substrate interface during locomotion of fibroblasts. *Biophys J* 76(4):2307-2316.

14. Barocas VH, Moon AG, & Tranquillo RT (1995) The fibroblast-populated collagen microsphere assay of cell traction force--Part 2: Measurement of the cell traction parameter. *J Biomech Eng* 117(2):161-170.

15. Napolitano AP, Chai P, Dean DM, & Morgan JR (2007) Dynamics of the self-assembly of complex cellular aggregates on micromolded nonadhesive hydrogels. *Tissue Eng* 13(8):2087-2094.

16. Foty RA, Pfleger CM, Forgacs G, & Steinberg MS (1996) Surface tensions of embryonic tissues predict their mutual envelopment behavior. *Development* 122(5):1611-1620.

17. Foty RA & Steinberg MS (2004) Cadherin-mediated cell-cell adhesion and tissue segregation in relation to malignancy. *Int J Dev Biol* 48(5-6):397-409.

18. Pokutta S & Weis WI (2007) Structure and mechanism of cadherins and catenins in cell-cell contacts. *Annu Rev Cell Dev Biol* 23:237-261.

19. Hartsock A & Nelson WJ (2008) Adherens and tight junctions: structure, function and connections to the actin cytoskeleton. *Biochim Biophys Acta* 1778(3):660-669.

20. Unwin PN (1987) Gap junction structure and the control of cell-to-cell communication. *Ciba Found Symp* 125:78-91.

21. Chrzanowska-Wodnicka M & Burridge K (1996) Rho-stimulated contractility drives the formation of stress fibers and focal adhesions. *J Cell Biol* 133(6):1403-1415.

22. Goeckeler ZM & Wysolmerski RB (1995) Myosin light chain kinase-regulated endothelial cell contraction: the relationship between isometric tension, actin polymerization, and myosin phosphorylation. *J Cell Biol* 130(3):613-627.

23. Omelchenko T*, et al.* (2001) Contact interactions between epitheliocytes and fibroblasts: formation of heterotypic cadherin-containing adhesion sites is accompanied by local cytoskeletal reorganization. *Proc Natl Acad Sci U S A* 98(15):8632-8637.

24. Katoh K, Kano Y, Amano M, Kaibuchi K, & Fujiwara K (2001) Stress fiber organization regulated by MLCK and Rho-kinase in cultured human fibroblasts. *Am J Physiol Cell Physiol* 280(6):C1669-1679.

25. Katoh K*, et al.* (2001) Rho-kinase--mediated contraction of isolated stress fibers. *J Cell Biol* 153(3):569-584.

26. Hayashi T & Carthew RW (2004) Surface mechanics mediate pattern formation in the developing retina. *Nature* 431(7009):647-652.

27. Sivasankar S, Brieher W, Lavrik N, Gumbiner B, & Leckband D (1999) Direct molecular force measurements of multiple adhesive interactions between cadherin ectodomains. *Proc Natl Acad Sci U S A* 96(21):11820-11824.

2.8. Figures

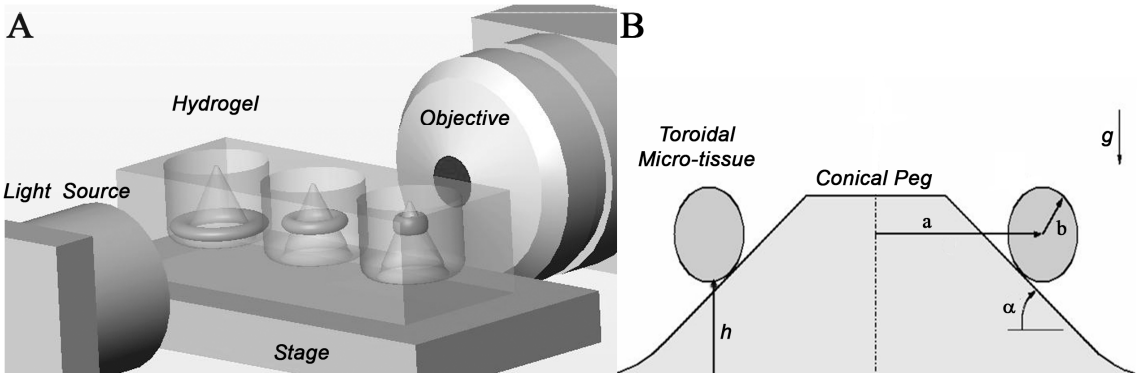

Figure 2-1: Schematic of experimental system to quantify the forces of self-assembly. (A) Mono-dispersed cells aggregate and form toroidal microtissues. The forces of self-assemble drive the toroid up the slope of the conical peg and this movement can be captured by side view microscopy. (B) Schematic of a cross section of a toroidal microtissue on a conical peg. Denoted are the height moved by the microtissue (*h*), the slope of the conical peg (*α*), the direction of gravity (*g*), and the major and minor radii (*a*) and (*b*), respectively.

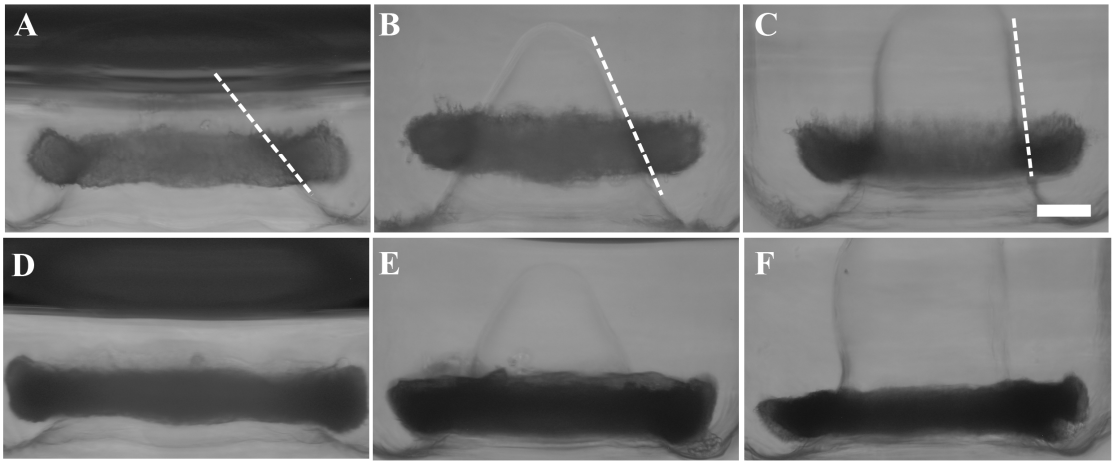

Figure 2-2: Self-assembling NHF and H35 toroids traveled up conical pegs at different rates. NHFs (A-C) and H35s (D-F) were seeded into micro-molded polyacrylamide gels with toroidal recesses and side view images obtained. Central conical pegs were designed with 55º (A & D) 65º (B & E) and 85º (C & F) slopes (dotted line added to accentuate slope). H35 microtissues reach the height that NHF microtissues reach in 2 hours (A-C) in 48 hours (D-F). Scale bar is 200 μm.

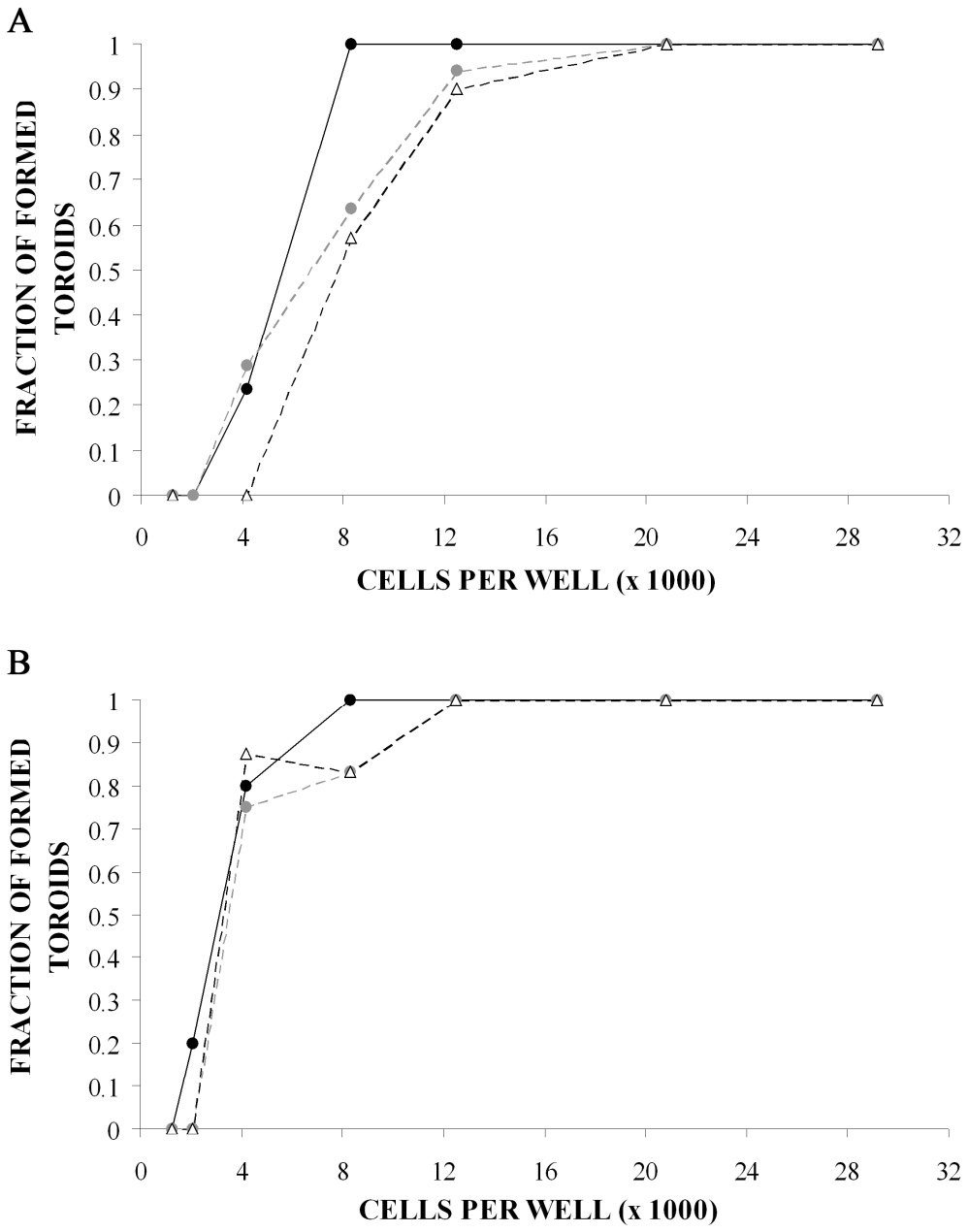

Figure 2-3: Toroid formation was cell number dependent. Different numbers of NHFs (A) and H35s (B) were seeded into toroidal wells with 55º (●), 65º (●), and 85º (Δ) slopes. The percentage of intact toroids was determined 17 hours after cell seeding. Sample size (n) is greater than 5 for all points.

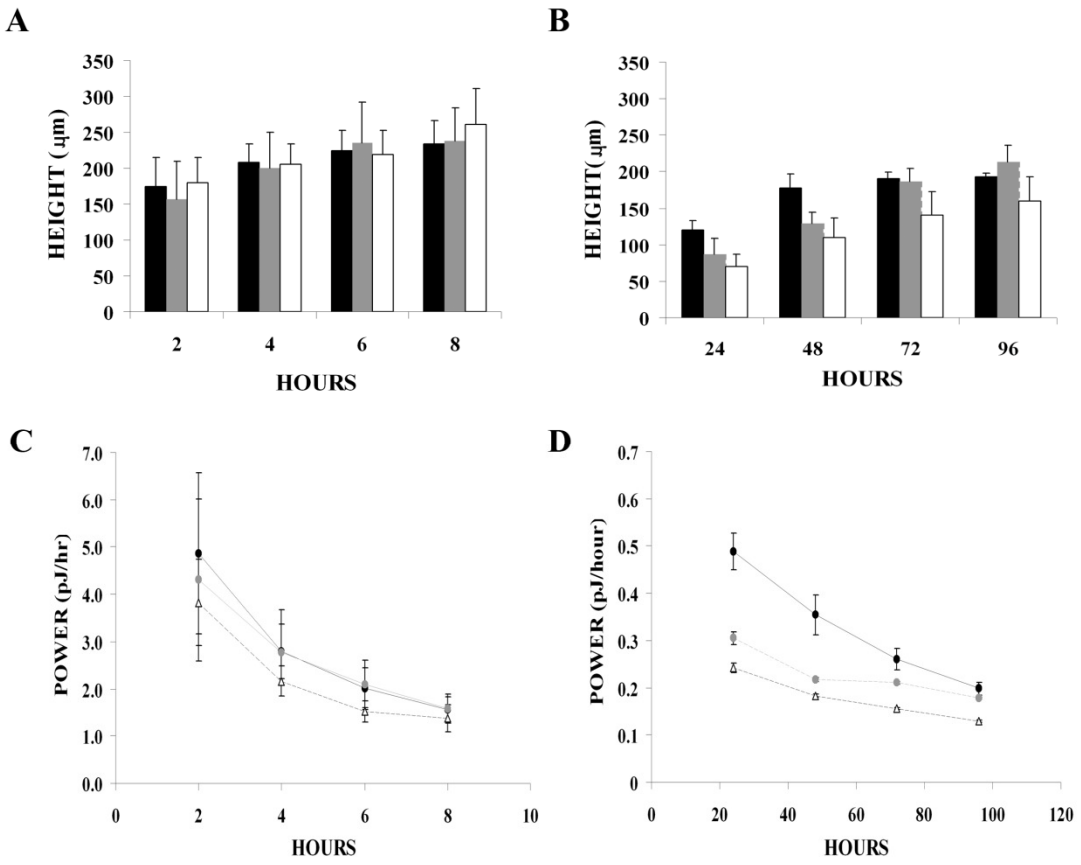

Figure 2-4: NHF toroid height and power output was independent of slope and of a much greater magnitude than that of the H35s. The distance traveled by the toroids up the conical pegs was measured as a function of time and peg slope of 85º (□), 65º (■), and 55º (■) for NHFs (A) and H35s (B). Movement of NHF toroids was rapid and differences between slopes were not statistically significant. Movement of H35 toroids was slower and the differences between the 85º and 65º and the 85º and 55º at 24 and 48 hours were statistically significant. At 72 and 96 hours differences between the 85º and 55º and the 65º and 55º were statistically significant. Cell power was calculated as a function of potential energy over time for NHF (C) and H35 (D) microtissues for the 55º (●), 65º (●), and 85º (Δ) slopes. The power output of H35 microtissues decreased substantially as the slope of the central peg increased ($p<0.05$). For NHFs n = 7, 9, and 6 for the 85º, 65º, and 55º, respectively. For H35s n = 9, 8, and 5 for the 85º, 65º, and 55º, respectively. Error bars are standard deviations.

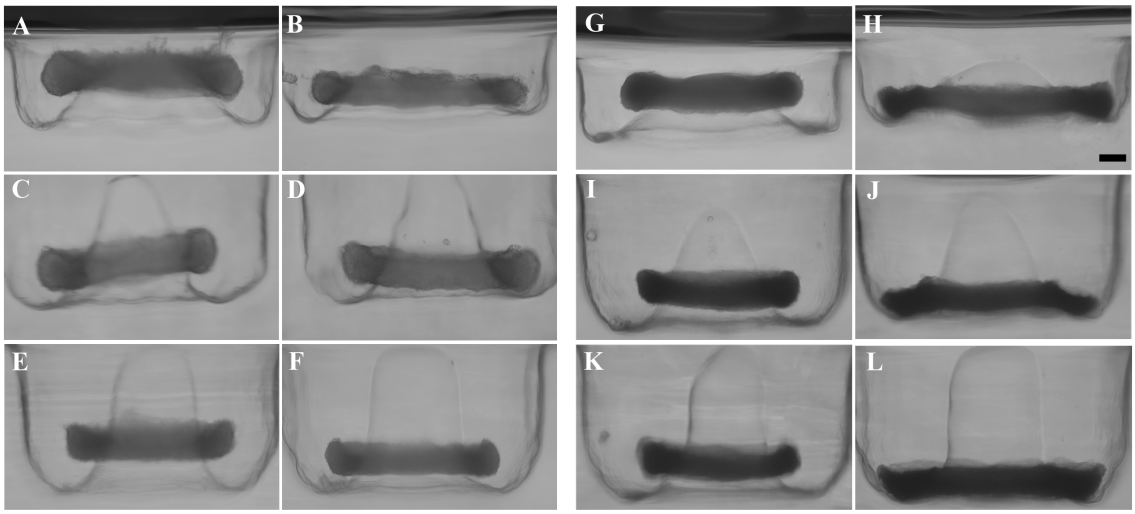

Figure 2-5: Inhibition of ROCK mediated contraction using Y-27632 impeded toroid motion up the conical peg of both NHFs and H35s. NHFs were treated with 0 (A, C, E) and 100 (B, D, F) μM Y-27632 and were seeded in drug equilibrated gels with 55º (A and B), 65º (C and D) and 85 º (E-F) slopes. As early as 2 hours, drug treated NHF sample were significantly lower on the peg than control samples. H35s were also treated with 0 (G, I, K) and 100 (H, J, L) μM Y-27632 and were seeded in drug equilibrated gels with 55º (G and H), 65º (I and J) and 85 º (K and L) slopes. The effect of drug treatment was visible after 24 hours. Scale bar = 200 μm.

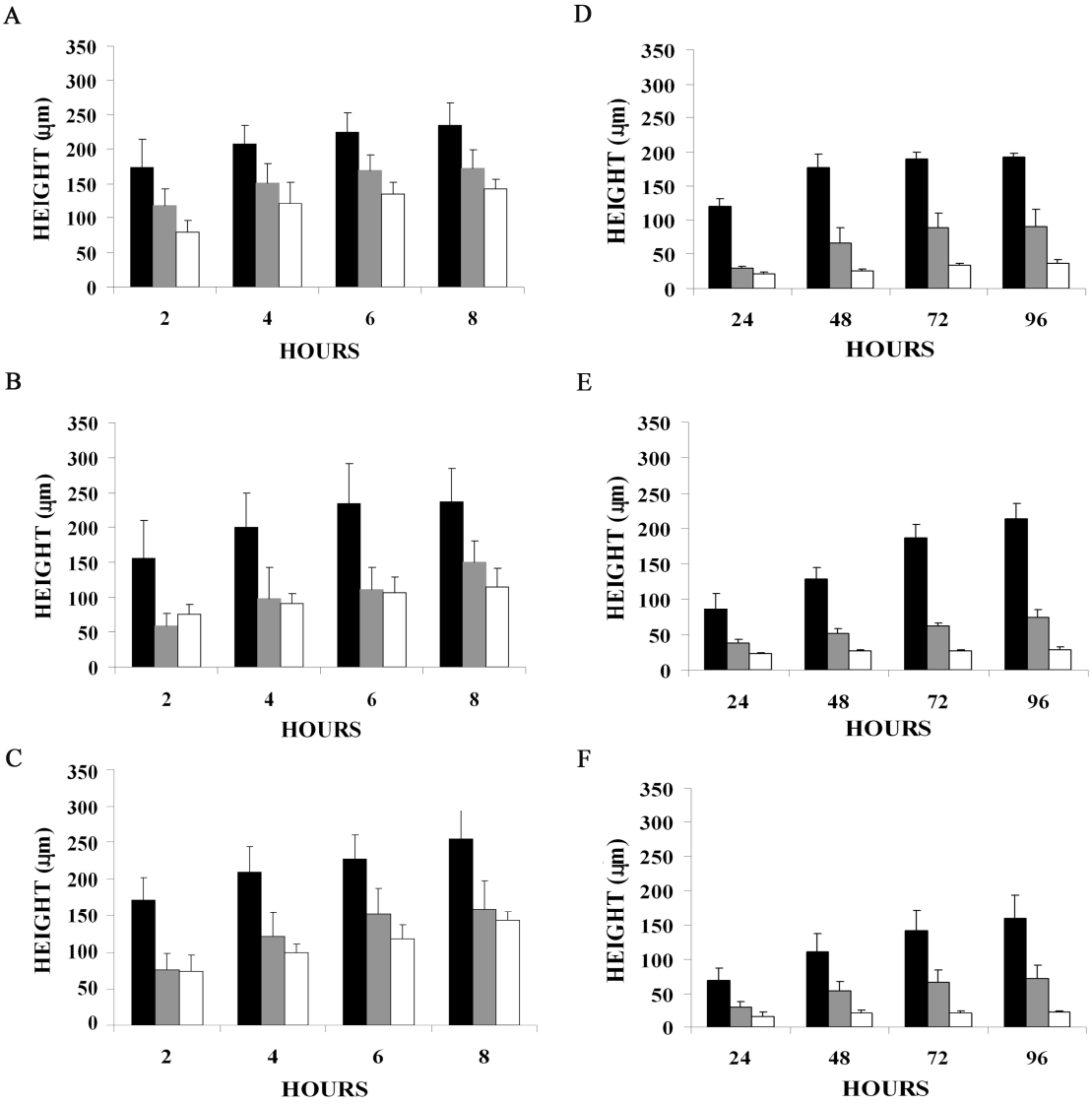

Figure 2-6: Toroid height was dependent on Y-27632 concentration for both NHFs and H35s. For all slopes, ROCK inhibition decreased the final height reached of NHF microtissues ($p<0.05$ between control and drug treated samples). The motion of NHF treated toroids was altered in a dose dependent manner for the 55º slope (A) as the dose was increased from 0 (■) to 10 (■) to 100 (□) µM. However, dose dependency was not observed for the 65º (B) and 85º (C) slopes as 10 µM of Y-27632 was sufficient to inhibit the motion of the microtissue to its fullest. ROCK inhibition altered the height achieved by H35 microtissues in a dose dependent manner for all slopes (D-F is 55º, 65º, and 85º, respectively) ($p<0.05$). Error bars represent standard deviations.

Table 2-1: NHF and H35 toroid power as a function of slope and Y-27632 concentration at 2 hours for NHFs and averaged over all time points for H35s.

NHF						
	85º		**65º**		**55º**	
Concentration Y-27632 (μM)	10	100	10	100	10	100
Power attributed to ROCK (pJ/hrs)	1.6	2.1	2.5	1.8	1.8	3.0
Decrease in Power (%)	42	53	57	41	36	60
H35						
	85 º		**65º**		**55º**	
Concentration Y-27632 (μM)	10	100	10	100	10	100
Power attributed to ROCK (pJ/hrs)	0.09 ±. 02	0.14±. 03	0.15 ±. 03	0.19 ±. 03	0.20 ±. 11	0.27 ±. 11
Decrease in Power (%)	51 ± 2	80 ± 3	65 ± 4	83 ± 5	59 ± 10	85 ± 2

CHAPTER 3

3. Mechano-Transduction is Enhanced by the Synergistic Action of Heterotypic Cell Interactions and TGF-β1.

Jacquelyn Youssef, Peng Chen, Vivek Shenoy, and Jeffrey R. Morgan

3.1.Abstract

Using planar substrates and three dimensional (3D) collagen gels, the field of mechano-transduction has focused on the role extracellular matrix stiffness, mechanical tension, and transforming growth factor-β1 (TGF-β1) in the generation of a more contractile fibroblast (NHF). Here, we have used 3D self-assembled microtissues, in which cell-cell interactions dominate, and a recently developed cell power assay to quantify the effects of TGF-β1 versus the heterotypic cell interface on the cell power exerted by mixed and pure NHF and hepatoctye (H35) microtissues. We found that TGF-β1 only doubled the power output of both pure NHF and H35 microtissues, whereas the heterotypic environment resulted in a 5 fold increase in cell power. Mixing TGF-β1 treated NHFs

with H35s demonstrated that the heterotypic environment and TGF-β1 synergistically increased cell power (22x) by maximizing heterotypic cell interactions. Using a mathematical simulation of stress generation and distribution, we show how tensile forces can be enhanced due to heterotypic cell interactions. These data render a new understanding of how heterotypic cell interactions may increase force generation of cells during wound healing.

3.2. Introduction

Cell-cell interactions are of wide fundamental importance to a myriad of processes that occur during development, wound healing, and metastasis. In addition to generating biochemical signals that trigger intracellular cascades, it is becoming increasingly clear that cell-cell interactions generate and sense mechanical forces and that these processes are equally important for controlling the behavior of cells and the surrounding tissue (1). This field of mechanobiology is examining the effects of various mechanical forces including adhesive forces (e.g., cadherins) and tensile forces, (e.g., myosin contraction) as well as the effects of the stiffness of cell types and their surrounding extracellular matrix (ECM). Compelling evidence has accumulated that mechanical forces not only mediate cell signaling, but also direct morphogenesis, cell migration and are altered in certain disease states such as metastasis and fibrosis (2-8).

Recently, we reported on an assay to quantify the different forces that drive the cell-cell adhesion and contraction that occurs when mono-dispersed cells self-assemble 3D microtissue (9). Using a systems biology approach, the assay measures the power expended by cells against gravity as the cells aggregate and form a toroid that ascends a cone shaped peg. We used the assay to quantify the power associated with the self-assembly of two cell types, normal human fibroblasts (NHF) and a rat hepatocyte cell line (H35), and to quantify the contribution of Rho kinase (ROCK) mediated cell contraction to the assembly of these cells. Here, we have used this assay to measure the

power behind the assembly of mixed (NHF/H35) microtissues and examined the role of heterotypic adhesion in generating cell tension and creating a more active cell. We identified the heterotypic environment as a very potent inducer of cell mediated tension and found its contribution to cell power to be significantly greater than that of a very well known inducer of contractility transforming growth factor-β1 (TGF-β1). Further demonstrating the importance of heterotypic interactions, we found that when heterotypic interactions were increased, by changing the ratio of NHFs to H35s and/or by treating the NHFs with TGF-β1, cell power was substantially increased. Mathematical simulation of stress distribution shows that tensile forces can be enhanced and further propagated over longer distances due to this heterotypic interface. With relevance to wound healing and fibrosis, these data imply that the initial heterotypic interactions between fibroblast and parenchymal cell maybe more important than TGF-β1 in the activation of fibroblast and the generation of tension in tissues.

3.3. Results

We measured the range of power exerted by increasing numbers of NHFs (>3fold) in a homotypic environment by seeding the cells into non-adhesive hydrogels with toroid recesses, each with a central cone (65° slope). Cells settled and formed cell-cell adhesions that drove the toroid shaped microtissue up the cone. We calculated the power necessary to move the NHF toroid up the cone as $P=\Delta W/\Delta t$, where ΔW is work performed against gravity to move a toroid of a known mass to a given height, and Δt is the time over which the work is performed. NHF toroid height (**Figure 3-1**) did not change with increasing NHF cell number (186 $\pm$ 19 μm, 2 hrs). Toroid power increased linearly as cell number increased, but power per NHF (cell power) was independent of cell number, with a peak cell power of 0.22 $\pm$. 02 fJ/hr (2 hrs) and an average cell power (over all time points) of 0.16 $\pm$. 03 fJ/hr.

To understand TGF-β1's effects on power, NHFs were treated with TGF-β1 and seeded into the toroid recesses. As early as two hours, height of the $NHF^{TGF-\beta1}$ toroid increased ~2 fold resulting in a significant increase in toroid power (9.82 $\pm$ 1.32 pJ/hr versus 5.08 $\pm$ 1.04 pJ/hr for controls) (**Figure 3-2**). Peak cell power (2 hrs) for $NHF^{TGF-\beta1}$ was 0.47 fJ/hr (2 hrs) and average cell power was 0.16 $\pm$ 0.21 fJ/hr. TGF-β1 also increased the power of homotypic toroids of H35s, a rat hepatocyte cell line. Untreated H35 toroids required 48 hours to move the same distance that NHF toroids moved in two hours (11). TGF-β1's effects on H35s were evident at 24 hours. $H35^{TGF-\beta1}$ toroid and cell power both

doubled to 0.45 $\pm$ 0.08 pJ/hr and 0.022 $\pm$ 0.004 fJ/hr, respectively, compared to untreated controls.

To examine cell power in a heterotypic environment, mixtures of NHFs and H35s were seeded with the total number of cells per toroid held constant (~21,000). Heterotypic toroids moved at different rates and reached different heights (**SI Figure 3-1**). Power of the heterotypic toroids decreased as the percentage of NHFs decreased and there was a delay to reach peak toroid power (**SI Figure 3-1**). To determine the effect of the heterotypic environment in conjunction to TGF-β1 treatment, $NHFs^{TGF\text{-}\beta1}$ were mixed with untreated H35s at varying ratios. All treated heterotypic toroids moved further up the peg with the 1:1, 1:10, and 1:20 samples moving 1.4, 4.4, and 6.3 times higher than their respective controls.

Interestingly, when NHFs or $NHFs^{TGF\text{-}\beta1}$ where seeded with H35s there was enhanced power. To make quantitative comparisons of the enhancement in cell power due to the heterotypic environment, we calculated the expected power of a toroid and compared it to its actual measured power to derive a value for enhanced toroid power (**Table 3-1**). For each mixture, since the power of a homotypic H35 toroid is undetectable in 8 hours, expected toroid power was calculated from the number of NHFs present in the mix multiplied by cell power value as measured in the corresponding homotypic environment (NHF or $NHF^{TGF\text{-}\beta1}$). The enhanced toroid power can be attributed to the increased activity of one of the two cell types in the mix (NHF or H35) or it can be attributed to the

heterotypic interface where both cell types interact. Since the homotypic H35 toroid power is undetectable at eight hours, we attributed all of the power of the heterotypic toroids to the NHFs in the mixture. Surprisingly, NHF cell power increased as the percentage of NHFs decreased, with the 1:10 ratio exerting the greatest peak power per NHF (1.17 $\pm$ 0.13 fJ/hr). This NHF cell power value in the heterotypic environment was 5 times greater than NHF cell power in the homotypic environment (100% NHFs; 0.24 fJ/hr), and 2.5 times greater than the effect of TGF-β1 treatment.

Likewise, $NHF^{TGF\text{-}\beta1}$ cell power increased in the heterotypic environment as the percentage of $NHF^{TGF\text{-}\beta1}$ decreased with the 1:20 mix exerting the greatest peak cell power (4.13 $\pm$ 1.22 fJ/hr) and the 1:10 mix exerting the greatest total cell power of 5.3 $\pm$ 1.32 fJ/hr between four and eight hours (**Figure 3-3**) meaning that the cell power of the $NHF^{TGF\text{-}\beta1}$ is increased by over 11 times in the heterotypic environment. When compared to untreated NHFs in a homotypic toroid, TGF-β1 treatment in conjunction with the heterotypic environment causes cell power to increase by over 22 times. Since TGF-β1 alone only doubles cell power, and the heterotypic environment alone only increases power five fold, the combination of these two factors is synergistic.

Alternatively, if the enhanced toroid power is attributed solely to the H35 and is distributed among all H35s in the toroid, the power per H35 is increased from near zero (homotypic environment) up to 0.23 fJ/hr (1:10 mix). This enhanced cell power value for an H35 is very large considering that baseline H35 cell power in a homotypic toroid is

very small (0.022 fJ/hr, detectable 24 hours post seeding) (9), and that such an enhanced value would be in the range of untreated NHFs in a pure NHF toroid.

For each of the mixes, there was a delay in toroid motion before peak power was reached. For homotypic NHF toroids, peak power was reached at the first time point (2 hours). As the percentage of NHFs in the mixes decreased, the time to reach peak power increased. To determine if this delay was due to the time for cells to self-sort, NHFs and H35s were fluorescently labeled and sorting was assessed (**SI Figure 3-2**). When the proportion of NHFs was high, the cells self-sorted within eight hours with NHFs forming a contiguous inner toroid with a circumferential coating of H35s. When the percentage of NHFs was reduced (< 1:4), the NHFs no longer sorted within the eight hours, nor formed a contiguous inner toroid, but were distributed throughout the toroid. In the 1:10 mix, sorting was evident after 24 hours, with the NHFs clustering into pockets centrally located in the toroid. Interestingly, this sorting was eliminated by treating the NHFs with TGF-β1 (**Figure 3-4**). Thus, neither sorting nor the formation of a contiguous NHF toroid is necessary (or the mechanism) for the movement of the toroid at low percentages of NHFs and TGF-β1 treatment inhibits self-sorting.

To investigate cytoskeletal changes in the heterotypic environment, toroids were stained for f-actin. Confocal images revealed that the gross cytoskeletal architecture were very different for homotypic versus heterotypic toroids (**Figure 3-5**). Homotypic NHF toroids had a continuous and dense f-actin network spanning the thickness of the toroid, whereas

homotypic H35 toroids had weak punctuate f-actin staining only at cell junctions. Heterotypic toroids (1:1 and 1:4) exhibited a dense f-actin network throughout the central NHF portion of the toroid up to the H35 junction. The 1:10 mix had dense f-actin networks focused around the NHFs that was randomly distributed through the thickness of the toroid, as NHFs had not yet sorted to the center.

H35s in direct contact with NHFs had a stronger f-actin signal than both H35s that were not in contact with NHFs and than H35s in a homotypic toroid. In the 1:20 mix, there were three different local cellular environments with distinct f-actin staining (**SI Figure 3-3**). One region had a high density of NHFs (I) with an f-actin network similar to that of a homotypic NHF toroid. Another region had a high density of H35s distant from NHFs (II) and an f-actin network similar to that of a homotypic H35 toroid. A third region had a single NHF surrounding a cluster of H35s (III) with a distinct cytoskeletal structure at the NHF/ H35 interface; a strong f-actin signal extending from the NHF to the nuclei of the surrounding H35s.

Tensile stress modeling demonstrated that the heterotypic environment increases stresses. In homotypic NHFs, the peg constrains the tissue from contracting leading to tensile stresses that decrease in magnitude radially outward from the surface of the peg (**Figure 3-6**). For the heterotypic tissue, in addition to the constraints from the peg, there is a new and more significant mechanism generating tensile stresses. Since the NHFs are surrounded by less contractile H35s, they cannot contract as much as in the homotypic

environment leading to the generation of much larger overall tension in the heterotypic environment. This tension decreases from the NHF boundary to the surrounding H35s. The tension in both the NHF and the *adjacent* H35s is significantly higher than the corresponding tension in the respective homotypic environments. Enhancement of mechanical tension also induces actomysosin activity in both cell types which would increase overall power in the heterotypic environment. This is consistent with the f-actin distribution which shows that the cortical actin of the H35 is rearranged and more aligned with the radial actin of the adjacent NHFs. Changes in tensile stresses in a heterotypic environment can be further enhanced for both the NHF and H35 by considering factors such as the shape of the NHF and differences in elastic stiffness of the cell types (**SI Table 3-1**). Modeling the NHF as an elongated ellipsoid (aspect ratio=5) doubles the tensile stress and if the stiffness of the H35s surrounding the NHFs is larger by a factor of five, than the tensile stress is increased by four fold.

3.4. Discussion

Cell-mediated mechanical forces, implicated in tissue remodeling and wound healing, are often the focus of pathological conditions such as fibrosis (10-12). Much work has focused on the contractile forces of cells embedded in an ECM and quantitative studies have helped to define the complex interplay between matrix composition and stiffness and the role of growth factors in regulating contractile forces in 3D analogs (10, 13-15). However in many circumstances, cells exert contractile forces on other cells and yet there is little quantitative understanding of the factors influencing direct cell-cell mechano-transduction. In fact, much of the work with cells in ECM analogs is assumed to be applicable to cell-cell interaction. Here, we quantify the forces of cell-cell interactions and show that the effect of heterotypic cell interactions is significantly greater than the effect of TGF-β1, a well-known inducer of cell contractility.

Previously, we have shown that mono-dispersed cells seeded onto non-adhesive hydrogels with toroidal shaped recesses aggregate and form a multi-cellular toroid that moves up the central cone (16). The complex cell-cell interactions driving this simple event were quantified in terms of power and shown to vary significantly between cell types. As a tool for quantifying the small forces of cell-cell aggregation, the toroid/cone assay does not interfere with cell function via contact and requires little if any calibration because it relies only on gravity, a well-characterized external force. Cell power is a quantitative systems biology measure of the multi-component system (mechanical,

chemical, and surface energy) that drives toroid motion up the cone. It is useful for making quantitative comparisons between cell types and quantifying the contributions of proteins or protein systems to the complex process of cell aggregation. We showed that over 50% of the power of a toroid could be reduced by blocking ROCK mediated contraction (9). Here, we have used the assay and cell power measurement to quantify the cell-cell mechanics that occur in mixes of two cell types in a 3D cellular environment.

In this study, when small numbers of NHFs were mixed with H35s to form heterotypic toroids, there was a significant increase in cell power due solely to the heterotypic environment. NHF cell power in the heterotypic environment was five times greater than in the homotypic environment. By comparison, the cell power of $NHF^{TGF\text{-}\beta1}$ increased only two fold when compared to cell power for the NHF in the homotypic environment. Interestingly, the maximal increase in NHF cell power was cell ratio dependent. NHF cell power in the 1:10 ratio was three times higher than the 1:1 ratio. The 1:10 ratio approximates the ideal 1:12 ratio in close spheres packing, where one sphere contacts twelve nearest neighbors maximizing heterotypic cell interactions. Within the toroid, we identified foci of heterotypic interactions by staining for f-actin. NHFs were located at these foci of f-actin staining and the signal was significantly stronger than areas of the toroid where H35 homotypic interactions predominated. The f-actin staining at these heterotypic foci was not confined to just the NHF but extended into neighboring H35s suggesting that they were experiencing increased tension and had a reorganized cytoskeleton (17).

Another interesting finding was that as the number of NHFs decreased, the time to reach peak power also decreased. For the 1:10 mix, power was undetectable for the first four hours and then rapidly rose to its peak power. One possibility is that this lag was necessary for NHFs to self-sort and form an inner toroid of NHFs within the heterotypic toroid. This was ruled out because these small numbers of NHFs are not able to form a contiguous toroid (9) and cell labeling showed that self-sorting did not coincide with peak power. Also, self-sorting of $NHFs^{TGF\text{-}\beta1}$ was reduced compared to untreated NHFs in the heterotypic environment. It is possible that the lag time is required for the changes to occur at the heterotypic interface that will result in increased power. NHFs may require time to sense and adapt to the increased load and/or make cytoskeletal changes at the heterotypic interface. Consistent with this possibility is the observation that after an hour of contact between a fibroblast and an epitheliocyte, the cortical actin of the epitheliocyte is disassembled and aligned with the radial actin of the adjacent fibroblast (17).

Although the cause of the increased power in the heterotypic environment is unclear, our data suggest that the changes are due to the heterotypic interface between NHF and H35s. The modeling data suggests that when highly contractile fibroblasts are surrounded by non-contractile H35s there is a significant enhancement in stress for both the NHFs and in the adjacent H35s compared to that in the homotypic environment. The increase in tensile stresses can lead to actomyosin recruitment (18) and the strong foci of f-actin staining suggests that the heterotypic interface causes a reorganization of the actin

cytoskeletons of the H35s surrounding NHFs. The H35 cortical actin that is now realigned would be part of a new contiguous hepato- fibro contractile unit with significantly more contractile force that could transmit stresses over greater distances. In this heterotypic contractile unit, both hepatocytes and fibroblast could make contributions to the enhanced power, perhaps via an increase in efficiency or recruitment of a power source that is only tapped through heterotypic interactions. Whatever the mechanism, the time for these changes is fairly rapid since the peak power of the 1:10 toroid is manifest at six hours. In addition to the influence of the heterotypic interface, we cannot rule out the possibility that NHFs secrete factors such as TGF-β1 that activate contractility of all H35s leading to increased power (19-21). This is probably a minor contribution because power did not significantly increase when H35s were treated with TGF-β1 (<8 hours) and f-actin staining is specifically increased at NHF/H35 interfaces and not H35/H35 interfaces in the same heterotypic toroid.

Although the effect of the heterotypic environment was greater than TGF-β1 treatment, their combined effects were synergistic and resulted in a 22 fold increase in cell power when compared to NHFs. TGF-β1 is pleiotropic and its actions on fibroblasts grown on 2D substrates and embedded in 3D gels have been well defined (22-26). TGF-β1's ability to induce contractility of the fibroblasts is certainly one means by which power is increased in the homotypic and heterotypic environments. However, increased contractility alone does not explain the synergistic action of TGF-β1 treatment and the heterotypic environment. One possible explanation is that $NHFs^{TGF\text{-}\beta1}$ engage in more

heterotypic interactions. This is supported by the observation that self-sorting of $NHFs^{TGF\text{-}\beta1}$ is reduced compared to untreated NHFs in the heterotypic environment. As self-sorting proceeds, NHFs segregate away from H35s and heterotypic interactions of higher power are exchanged with homotypic interactions of lower power. By inhibiting self-sorting, TGF-β1 treatment sustains the heterotypic interactions that lead to the most significant increase in power. This was evident in the 1:10 sample for which there was not a single, but two peaks in power.

The nature of the heterotypic interactions and how they give rise to increased power is unclear. Whereas, homotypic interactions of fibroblasts are well characterized and include the formation of large, stable cell-cell adherens junctions that transmit contractile stress (6) and cadherin expression that changes from N-cadherin to stronger OB cadherins (27). In addition to being mechanically coupled, fibroblasts engaged in homotypic interactions that are also electrochemically coupled via gap junctions (6). It remains to be determined how the heterotypic interface is coupled and how this coupling differs from the homotypic interface.

Changes to the mechanical environment after tissue injury is an immediate and significant ongoing stimulus for scarring and fibrosis of numerous organs and tissues. Soon after tissue injury, fibroblasts migrate out of the stable, stress shielding ECM and into a heterotypic environment where it interfaces for the first time with parenchymal cells and the ratio of cell-cell interactions compared to cell-ECM interactions increase

(6). Our data suggest that the heterotypic interface is a stimulus significantly greater than TGF-β1 and that it may serve to increase contractility and/or be an initial event activating the fibroblast which in turn increases stress in the parenchyma. TGF-β1's role in this early stage is synergistic and would serve to sustain and increase these heterotypic interactions. Inhibiting these very early events at the heterotypic interface may be a useful target for an anti-fibrotic strategy.

3.5. Materials and Methods

Micro-mold design and gel casting

Toroid molds suitable for side view microcopy were designed as previously described (9). Toroid molds were designed using the computer aided design (CAD) software Solid Works (Solid Works Corporation, Concord, MA). The mold was designed with 12 features to create wells. Each feature is a rounded edged (350 μm in diameter) cylinder (1.1 mm) with a cone indent in the center. The slope of the central cone was 65º and 650 μm in diameter. CAD files were used to produce thermowax molds with a rapid prototyping machine (3D Systems Corporation, Valencia, CA).

Wax molds were used to cast 13% polyacrylamide gels. Gels were removed from wax molds and transferred to six well culture plates. Each of the resulting wells is a circular trough confined by the hydrogel wall at the outer edge of the trough and by a conical peg on the inner edge of the trough. The gels were rinsed with fresh culture medium and then equilibrated overnight at 37ºC in 4 ml of DMEM supplemented with 10% fetal bovine serum (FBS) and 1% penicillin/streptomycin (pen/strep). After equilibration, the medium was removed, and the gels were rinsed with fresh medium.

Cell culture and gel seeding

NHFs (passage 4-10), derived from neonatal foreskins, and H35s (passage 5-11) were grown in T-175 flasks in DMEM with 10% FBS and 1% pen/strep at 37ºC and 10% CO_2. Cells were removed from flasks using a standard trypsin process. Briefly, cells were

exposed to 0.05% trypsin for 10 minutes, quenched with serum containing medium, spun down at 800 rpm for 6 minutes, resuspended in a known volume of medium, and counted using a hemocytometer. 70 µl of cell solution was added to each hydrogel. After 30 minutes, 4 ml of fresh medium was added to each of the wells. After seeding, images of the samples were taken every 2 hours for 8 hours. Pure NHF microtissues were seeded with 10,500, 21,000, 25,000 or 35,000 cells/well. Heterotypic microtissues were seeded at ratios of 1:1, 2:3, 1:4;1:6, 1:10, 1:16, and 1:20 (NHF:H35). The seeding per well for heterotypic samples was kept constant at 21,000 cells/well. For TGF-β1 experiments, NHFs and H35s were incubated for 48 hours in DMEM with 10% FBS, 1% penn/strep and 5 ng/ml Human Recombinant TGF-β1, passed according to standard protocol, and seeded at 21,000 cells/well.

For sorting experiments, NHFs and H35s were incubated with 2.5 µM CellTracker^{TM} Red CMPTX and CellTracker^{TM} Green CMFDA, respectively, in serum free media for 30 minutes. After incubation, the dye was aspirated and the cells equilibrated in serum media for 1 hour prior to passing. For NHF$^{TGF-\beta1}$:H35 sorting experiments NHFs were incubated for 48 hours in DMEM with 10% FBS, 1% penn/strep and 5 ng/ml Human Recombinant TGF-β1. After incubation the NHF$^{TGF-\beta1}$ and H35s were fluorescently labeled and passed as previously described.

Microscopy and Image analysis

Conventional view fluorescent and phase images were captured using Carl Zeiss Axio Observer Z1 with an AxioCam Mrm camera (Carl Zeiss MicroImaging, Thornwood, NY). To capture side view images a Mitutoyo FS-110 microscope was modified to lie on its back and a translational stage was added to hold samples. Samples were imaged in bright field through the eyepiece of the microscope. ImageJ Software (Rasband, W.S., ImageJ, NIH) was used measure the height of the toroid, the major radius, and the minor radius of the toroid.

Immunohistochemistry and Confocal Microscopy

Prior to passing, NHFs were incubated with CellTracker^{TM} Red CMPTX in serum free DMEM for 30 minutes. Fluorescently labeled NHFs were seeded with unlabeled H35s. 8 hours post-seeding microtissues were fixed overnight in 4% formaldehyde. Samples were then rinsed 3 times with 0.002% Triton X-100 and permeabilized for 6 hours in 0.5% Triton X-100. Microtissues were then incubated with 1 ml of 300 nM DAPI dihydrochloride and Oregon Green 488 Phalloidin (Invitrogen, Carlsbad, CA) for 1 hour. Confocal images were captured with a Zeiss LSM 510 confocal microscope.

Principle Stress Modeling

To model the tensile stresses generated by the contractility of the NHFs in homotypic and heterotypic environments, we carried out finite element simulations by assuming linear elastic constitutive relations (Young's modulus E = 2 kPa and Poission's ratio = 0.5 (5))

for both the NHFs and H35s. The stresses in the toroids were computed in the finite element framework using the package ABAQUS v6.10 (SIMULIA, Providence, RI). Since there are no constraints along the z-direction and as the thicknesses of cell aggregates are smaller than their lateral dimensions in the x-y plane, plane stress elements CPS3 were used in all the finite element simulations. The peg was assumed to be rigid and the contact between the peg and the cells was modeled using normal hard-contact elements. From a mechanistic perspective, the deformation and stresses created in an actin network by myosin motors can be modeled by treating the motors as force dipoles (28-31). This is because the motors exert equal but opposite forces along the actin filaments. When a large number of these motors are involved as in the case of cell aggregates, a coarse-grained description based on contractile strain, which gives the measure of the dipole strength per unit volume can be adopted. Mathematically, the elastic fields arising from the contractile strain due to myosin motors is similar to the fields created by sources of internal stress in solid materials, for example temperature fields, where thermal strain leads to the body forces (32). In our simulations, thermal strain induced by the spatially varying temperature fields, implemented in ABAQUS v6.10, is used to model the contractility in the cell aggregates. In all the simulations, the contractile strain in NHFs is assumed to be uniform and isotropic (magnitude = 0.01) while the contractile strain in the H35s is assumed to be negligible. To investigate the effect of shape and stiffness of the cells on the enhancement of stresses in heterotypic mixes, we considered the changes in stress with NHF aspect ratios of 2 and 5 (major/minor radius) and H35 stiffness increased 5 fold.

3.6. Acknowledgments

This work was funded, in part by the MRSEC Program of the National Science Foundation under award DMR-0520651, the NIRT Program under award DMI-0506661, NSF CMMI-0825185 and NIH R01EB008664-01A1.

3.7. References

1. Chen CS, Tan J, & Tien J (2004) Mechanotransduction at cell-matrix and cell-cell contacts. *Annu Rev Biomed Eng* 6:275-302.
2. Makrilia N, Kollias A, Manolopoulos L, & Syrigos K (2009) Cell adhesion molecules: role and clinical significance in cancer. *Cancer Invest* 27(10):1023-1037.
3. Ingber DE (2006) Mechanical control of tissue morphogenesis during embryological development. *Int J Dev Biol* 50(2-3):255-266.
4. Krieg M*, et al.* (2008) Tensile forces govern germ-layer organization in zebrafish. *Nat Cell Biol* 10(4):429-436.
5. Discher DE, Janmey P, & Wang YL (2005) Tissue cells feel and respond to the stiffness of their substrate. *Science* 310(5751):1139-1143.
6. Hinz B & Gabbiani G (2003) Cell-matrix and cell-cell contacts of myofibroblasts: role in connective tissue remodeling. *Thromb Haemost* 90(6):993-1002.
7. Albelda SM (1993) Role of integrins and other cell adhesion molecules in tumor progression and metastasis. *Lab Invest* 68(1):4-17.

8. Mammoto T & Ingber DE (2010) Mechanical control of tissue and organ development. *Development* 137(9):1407-1420.

9. Youssef J, Nurse AK, Freund LB, & Morgan JR (2011) Quantification of the forces driving self-assembly of three-dimensional microtissues. *Proc Natl Acad Sci U S A*.

10. Tomasek JJ, Gabbiani G, Hinz B, Chaponnier C, & Brown RA (2002) Myofibroblasts and mechano-regulation of connective tissue remodelling. *Nat Rev Mol Cell Biol* 3(5):349-363.

11. Desmouliere A, Chaponnier C, & Gabbiani G (2005) Tissue repair, contraction, and the myofibroblast. *Wound Repair Regen* 13(1):7-12.

12. Gabbiani G (2003) The myofibroblast in wound healing and fibrocontractive diseases. *J Pathol* 200(4):500-503.

13. Hinz B (2009) Tissue stiffness, latent TGF-beta1 activation, and mechanical signal transduction: implications for the pathogenesis and treatment of fibrosis. *Curr Rheumatol Rep* 11(2):120-126.

14. Hinz B, Celetta G, Tomasek JJ, Gabbiani G, & Chaponnier C (2001) Alpha-smooth muscle actin expression upregulates fibroblast contractile activity. *Mol Biol Cell* 12(9):2730-2741.

15. Freyman TM, Yannas IV, Yokoo R, & Gibson LJ (2001) Fibroblast contraction of a collagen-GAG matrix. *Biomaterials* 22(21):2883-2891.

16. Dean DM, Napolitano AP, Youssef J, & Morgan JR (2007) Rods, tori, and honeycombs: the directed self-assembly of microtissues with prescribed microscale geometries. *Faseb J* 21(14):4005-4012.

17. Omelchenko T*, et al.* (2001) Contact interactions between epitheliocytes and fibroblasts: formation of heterotypic cadherin-containing adhesion sites is accompanied by local cytoskeletal reorganization. *Proc Natl Acad Sci U S A* 98(15):8632-8637.

18. Fernandez-Gonzalez R & Zallen JA (2009) Cell mechanics and feedback regulation of actomyosin networks. *Sci Signal* 2(101):pe78.

19. Desmouliere A, Geinoz A, Gabbiani F, & Gabbiani G (1993) Transforming growth factor-beta 1 induces alpha-smooth muscle actin expression in granulation tissue myofibroblasts and in quiescent and growing cultured fibroblasts. *J Cell Biol* 122(1):103-111.

20. Lamouille S & Derynck R (2007) Cell size and invasion in TGF-beta-induced epithelial to mesenchymal transition is regulated by activation of the mTOR pathway. *J Cell Biol* 178(3):437-451.

21. Birchmeier C & Gherardi E (1998) Developmental roles of HGF/SF and its receptor, the c-Met tyrosine kinase. *Trends Cell Biol* 8(10):404-410.

22. Park JS, Kim JY, Cho JY, Kang JS, & Yu YH (2000) Epidermal growth factor (EGF) antagonizes transforming growth factor (TGF)-beta1-induced collagen lattice contraction by human skin fibroblasts. *Biol Pharm Bull* 23(12):1517-1520.

23. Montesano R & Orci L (1988) Transforming growth factor beta stimulates collagen-matrix contraction by fibroblasts: implications for wound healing. *Proc Natl Acad Sci U S A* 85(13):4894-4897.

24. Chen J, Li H, SundarRaj N, & Wang JH (2007) Alpha-smooth muscle actin expression enhances cell traction force. *Cell Motil Cytoskeleton* 64(4):248-257.

25. Roberts AB, Heine UI, Flanders KC, & Sporn MB (1990) Transforming growth factor-beta. Major role in regulation of extracellular matrix. *Ann N Y Acad Sci* 580:225-232.

26. Vaughan MB, Howard EW, & Tomasek JJ (2000) Transforming growth factor-beta1 promotes the morphological and functional differentiation of the myofibroblast. *Exp Cell Res* 257(1):180-189.

27. Hinz B, Pittet P, Smith-Clerc J, Chaponnier C, & Meister JJ (2004) Myofibroblast development is characterized by specific cell-cell adherens junctions. *Mol Biol Cell* 15(9):4310-4320.

28. Zemel A & Safran SA (2007) Active self-polarization of contractile cells in asymmetrically shaped domains. *Phys Rev E Stat Nonlin Soft Matter Phys* 76(2 Pt 1):021905.

29. Carlsson AE (2006) Contractile stress generation by actomyosin gels. *Phys Rev E Stat Nonlin Soft Matter Phys* 74(5 Pt 1):051912.

30. MacKintosh FC & Levine AJ (2008) Nonequilibrium mechanics and dynamics of motor-activated gels. *Phys Rev Lett* 100(1):018104.

31. Chen P & Shenoy VB (2010) Strain stiffening induced by molecular motors in active crosslinked biopolymer networks *Soft Matter* 2(2):355-358.

32. Timoshenko SP & FGoodier JN (1970) *Theory of Elasticity* (McGraw-Hill Companies, Inc) 3 Ed.

3.8. Figures

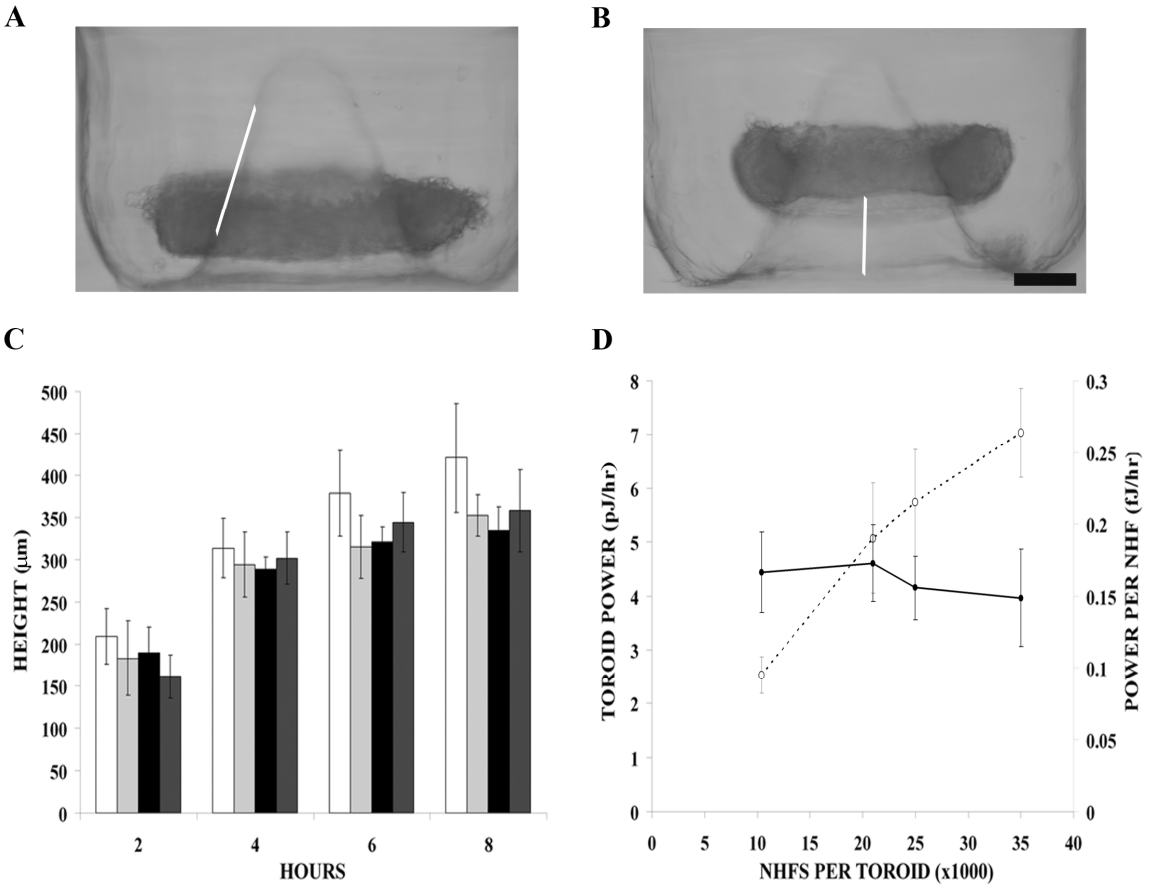

Figure 3-1: Toroid height and NHF cell power were constant regardless of cell number. NHFs were seeded into toroid micro-molds with increasing cells per toroid. Side view images of the toroids were taken, at 2 (A) and 4 hours (B). As early as 2 hours the toroid had begun to move up the cone (line added to show slope) and continued up the cone. Toroid height was measured from the bottom of the well to bottom of the toroid at 2 hour intervals for 8 hours for 10,500 (□); 21,000(■); 25,000 (■); and 35,000 (■) cells per toroid (C). Toroid power (open circles) was directly proportional to the number of cells within the toroid (R^2=0.97) while cell power (closed circles) was constant over the range of cell numbers tested. Scale bar is 200 µm.

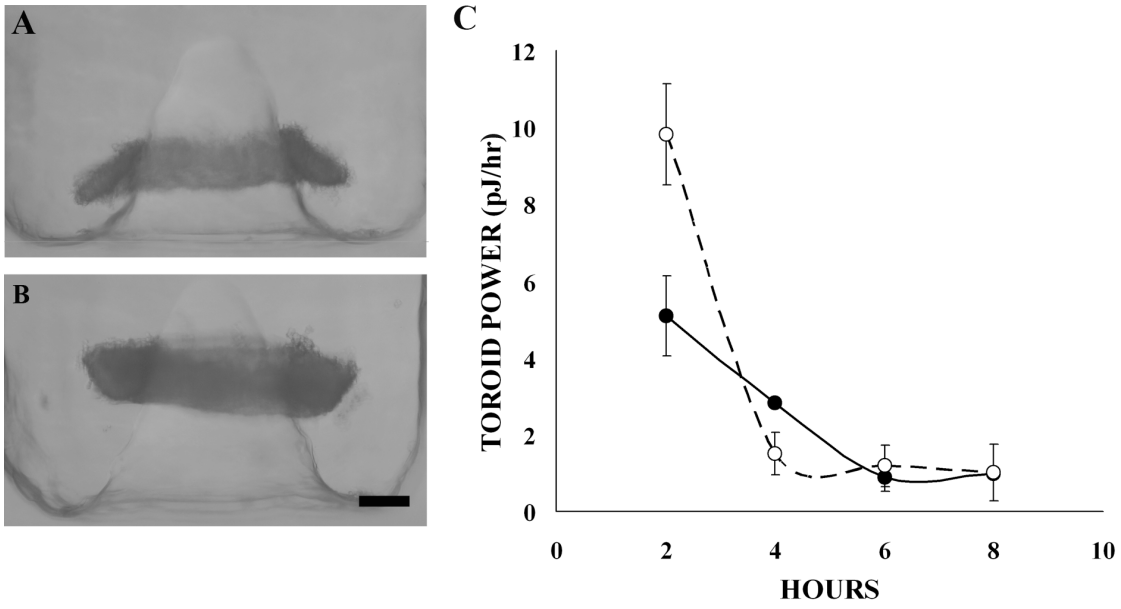

Figure 3-2: TGF-β1 treatment increased NHF power. NHFs were treated for 48 hours in 5 ng/ml TGF-β1 and then seeded into toroid recess. After 2 hours, toroids of NHFs treated with TGF-β1 (B) moved twice as far up the peg compared to untreated NHFs (A). (C)TGF-β1 treatment (open circles) resulted in doubling in cell power relative to the untreated controls (closed circles). Scale bar is 200 μm.

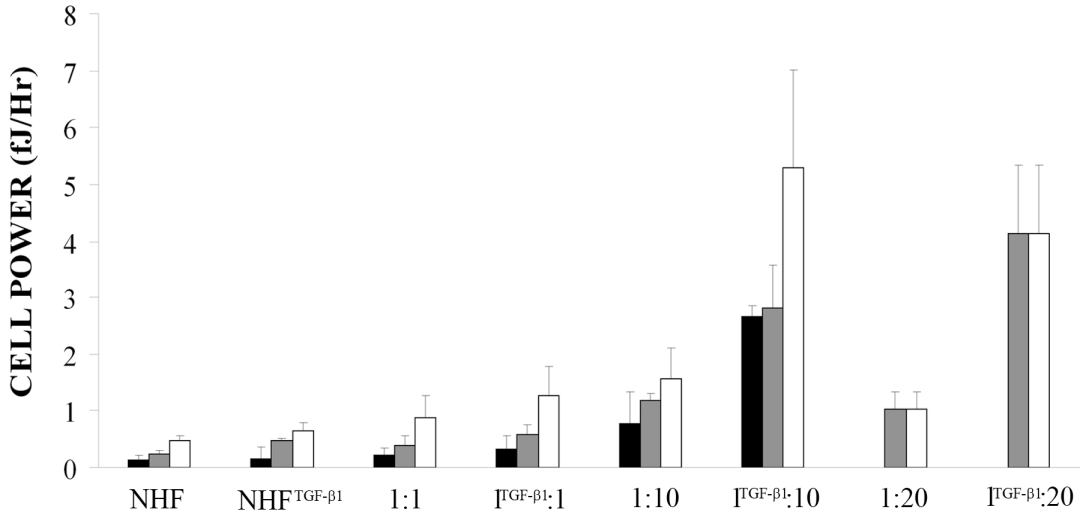

Figure 3-3: NHF Cell power increased with TGF-β1 and the heterotypic environment. Average cell power (black bars), peak cell power (gray bars) and total cell power (white bars) were calculated for each sample with the assumption that all power is generated by the NHFs. Average cell power was calculated as the mean power per cell value for each sample (over the time in which the samples exerted power), peak cell power is the maximum cell power output of each sample at a single time point, and total cell power is the sum of the cell power over the duration of the experiment.

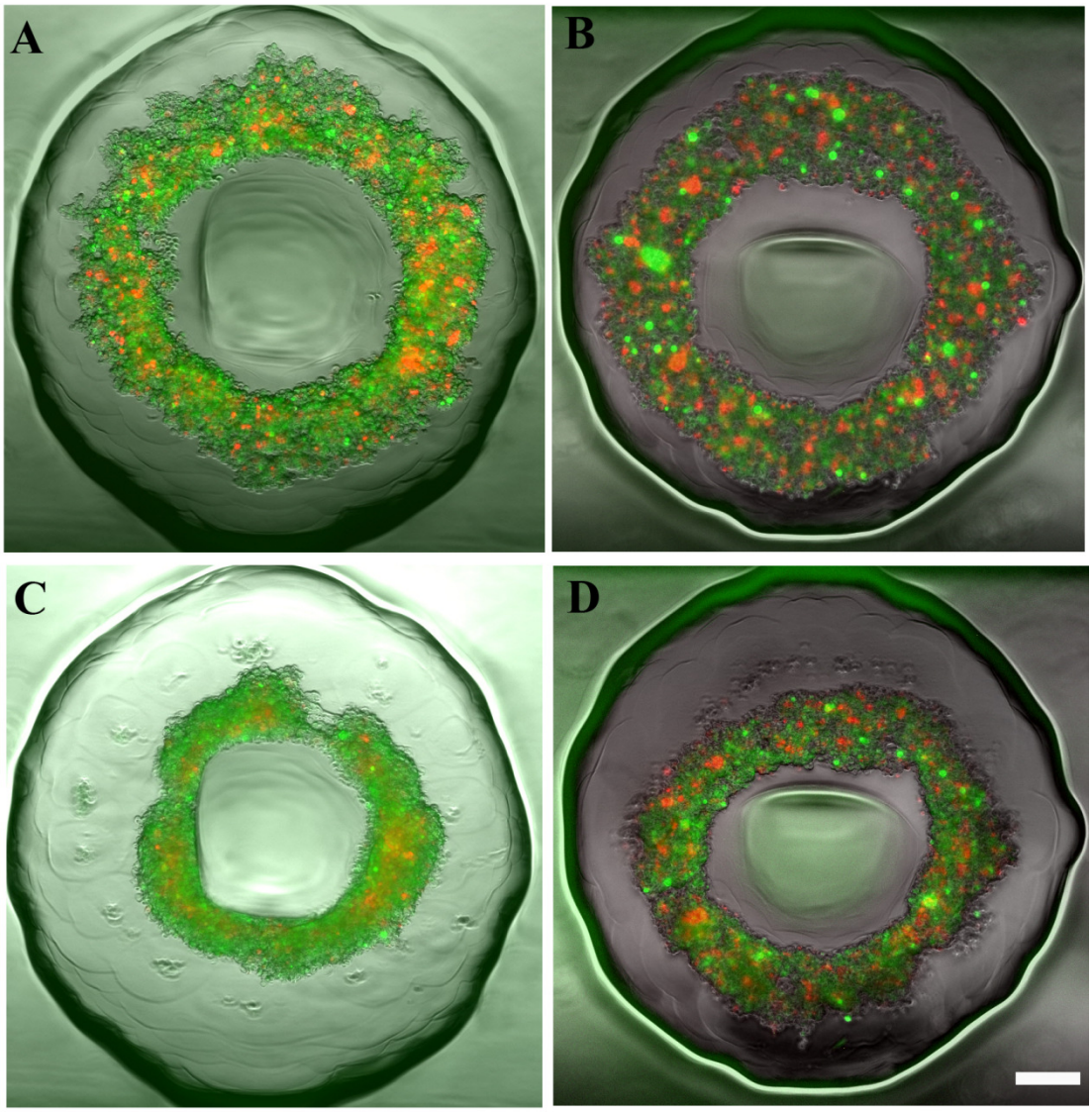

Figure 3-4: Delay in peak power was not related to the time to self-sort and TGF-β1 treatment decreased sorting. NHF/ $NHF^{TGF-\beta1}$ (red) and H35s (green) were seeded at a 1:10 ratio. For untreated samples (A & C), sorting is visible at 24 hours (C) with NHFs (red) taking the interior position and H35s (green) the exterior; but, sorting was absent in the peak power time (A). TGF-β1 treatment of NHFs prevented sorting (B & D) as sorting was absent at both the peak power time (B) and 24 hour time point (D). Scale bar is 200 μm

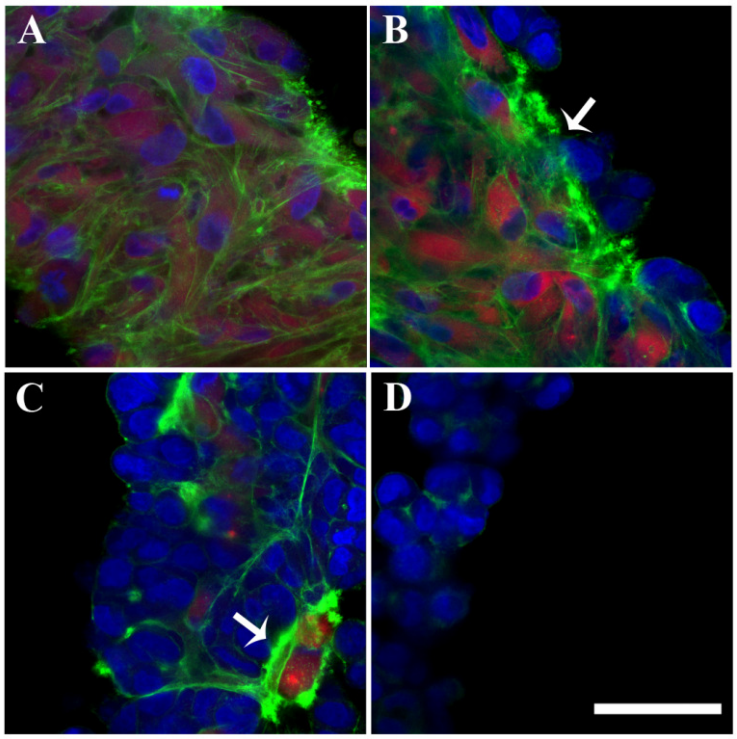

Figure 3-5: Cytoskeletal architecture was altered in the heterotypic environment. Pure NHF (A), 1:1 (B), 1:10 (C), and pure H35 (D) microtissues were fixed and stained after 8 hours. The nuclei and f-actin of all cells was labeled with DAPI (blue) and phalloidin (green), respectively and NHFs were labeled with CellTracker™ Red prior to self-assembly. H35s are identified as cells with a blue nuclei without red staining. Pure NHF microtissues had a dense, continuous f-actin network while pure H35 microtissues had a week punctuate f-actin signal. In heterotypic mixes, there was an enhanced f-actin signal at the junction between NHFs and H35s which met the nuclei of the H35. Scale bar is 50 μm.

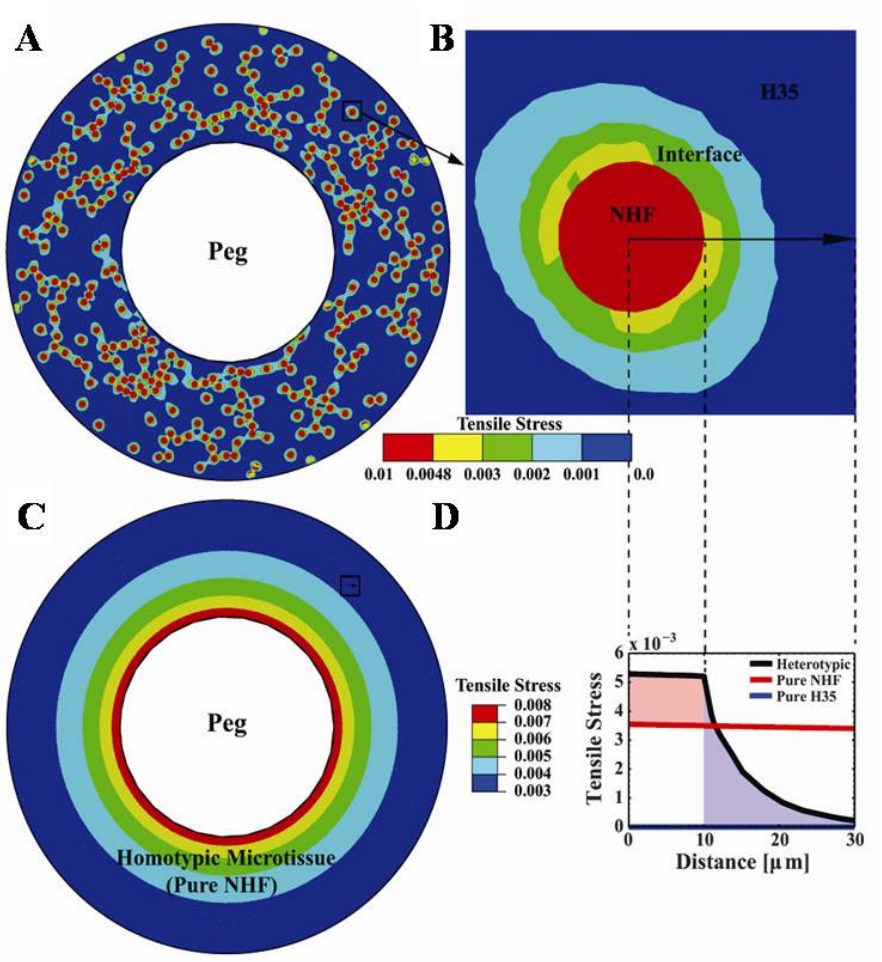

Figure 3-6: Simulation of stress distribution in heterotypic microtissues demonstrates that the heterotypic environment increased stress in the NHF and the surrounding H35s. For the 1:10 ratio (A & B), NHFs (red circles) are randomly distributed with the H35s in a toroid with peg and toroid radii of 325 μm and 675 μm, respectively (A & B). The contractility of NHFs results in tension in the NHF, the NHF/H35 heterotypic interfacial region and in the H35. The variation of the tensile stresses near one of the NHFs surrounded by H35s (black square in (A)) is plotted (B). The tension induced by the contractility of NHFs decreases from the interface of the NHF with the surrounding H35s. Note that the tension in the heterotypic interface region is much larger than in the surrounding H35 region (blue). The tensile stresses in homotypic microtissues (C) decrease radially from the peg and are uniform circumferentially. (D) The tensile stresses of heterotypic and homotypic microtissues in the same location (indicated by the black squares) are compared: The black curve corresponds to stresses in the heterotypic tissue, while the red and blue curves represent stresses in homotypic NHF and H35 tissues of the same dimensions. The red and blue shaded regions (D) indicate the enhancement in tension for the NHFs and H35s in the heterotypic tissue, compared to the tension in the corresponding homotypic environments. Tensile stresses we plot correspond to the maximum in-plane principal stress, and are normalized by the elastic modulus of cells. Arrow in (B) denotes the path along which the distance in (D) is measured. The decay of the tension (D) in the heterotypic interface region is consistent with the F-actin distribution shown in Figure 3-5.

Table 3-1: Heterotypic toroids have enhanced power. Measured toroid power was the toroid power exhibited at the time of peak power for each of the samples (1:10 is the combination of 6 and 8 hours as there were two peaks in power). Expected toroid power equals the power per NHF (homotypic toroid) or TGF-β treated NHF multiplied by the number of NHFs in the mixed toroid. Enhanced toroid power equals the difference between the measured toroid power and the expected toroid power. When treated with TGF-β and in the heterotypic environment NHFs are 22x more powerful if enhanced power is distributed to NHFs. If enhanced power is distributed to the H35, the H35 has enhanced power in the range of untreated NHFs.

Heterotypic Toroids	Measured Toroid Power (pJ/hr)	Expected Toroid Power (pJ/hr)	Enhanced Toroid Power (pJ/hr)	NHF has Enhanced Power (fJ/hr per NHF)	Relative Increase in NHF Cell Power	H35 has Enhanced Power (fJ/hr per H35)
1:1 (NHF:H35)	4.02	2.50	1.52	0.39	1.6x	0.15
1:10 (NHF:H35)	2.21	0.45	1.75	1.17	4.9x	0.09
1:20 (NHF:H35)	1.01	0.24	0.77	1.02	4.2x	0.04
1:1 ($NHF^{TGF-\beta}$: H35)	6.05	4.90	1.16	0.58	2.4x	0.11
1:10 ($NHF^{TGF-\beta}$: H35)	5.30	0.89	4.41	5.30	22.1x	0.23
1:20 ($NHF^{TGF-\beta}$: H35)	4.10	0.47	3.63	4.13	17.2x	0.18

3.9. Supplementary Materials

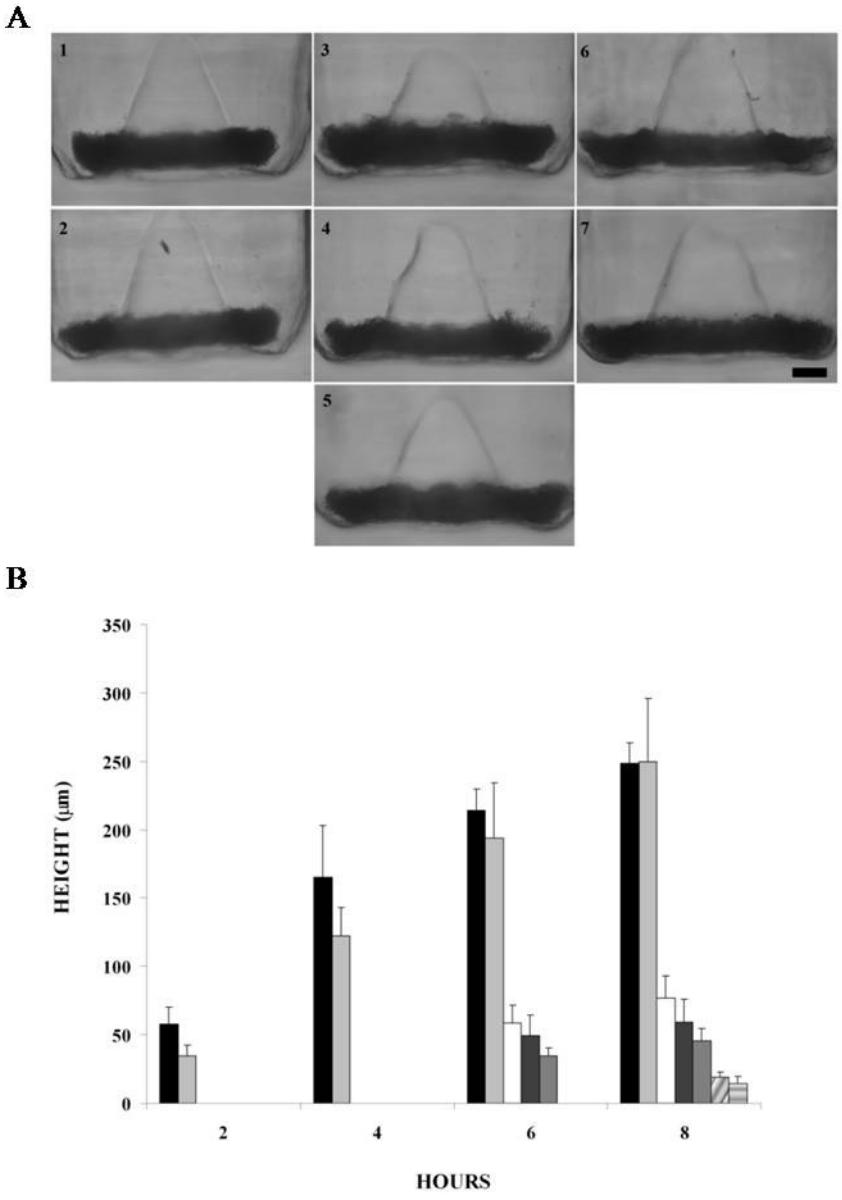

SI Figure 3-1: Heterotypic mixtures of NHFs and H35s self-assemble into toroids and move up the conical pegs at different rates. 1:1 (a) and 2:3 (b) samples after 2 hours 1:4 (c), 1:6 (d), and 1:10 (e) samples after 6 hours and 1:16(f) and 1:20 (g) samples after 8 hours. Toroid height (h) increased over time and decreased as ratio of NHFs to H35s decreased for the 1:1 (■), 2:3 (■), 1:4 (□), 1:6 (■), 1:10 (■), 1:16 (diagonal stripes), and 1:20 (horizontal stripes) samples. Scale bar is 200 μm.

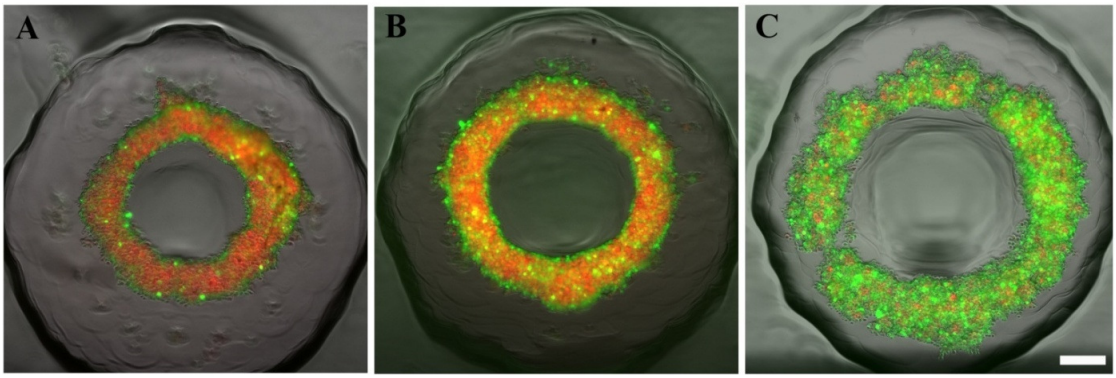

SI Figure 3-2: NHFs self-sort with H35s within 4 hours for ratios greater than 1:4. NHFs (red) were seeded with H35s (green) and self-sorting was evaluated. For the 1:1 (A) and the 2:3 (B) ratios (NHF:H35) sorting was present at four hours. However, when the ratio was greater than 1:4 (C) self-sorting was to a lesser extent or absent. Scale bar is 200 μm.

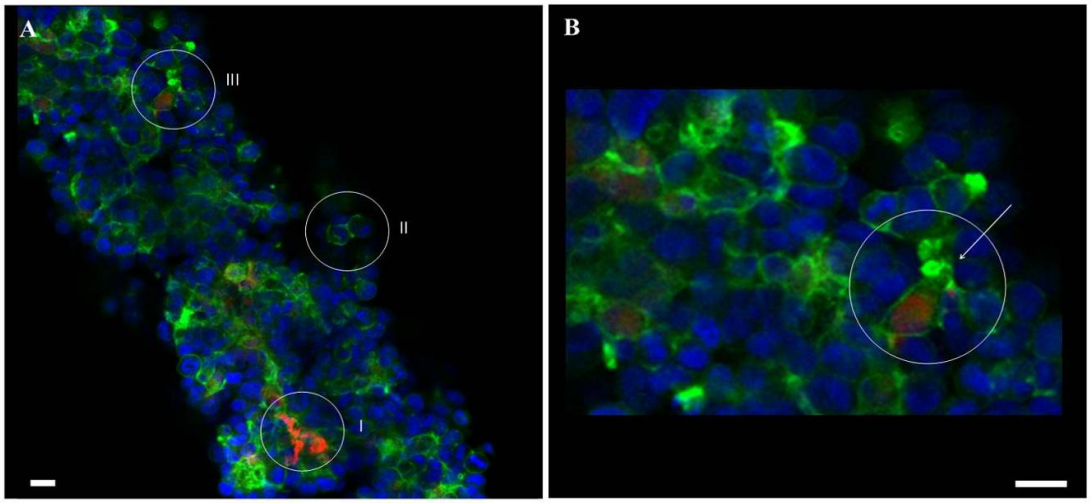

SI Figure 3-3: F-actin signal is strong in areas where H35s contact NHFs. Heterotypic toroids (1:10) were fixed at 8 hours and nuclei stained with DAPI (blue) and f-actin with phalloidin (green). NHFs were labeled with Cell Tracker Red prior to self-assembly and H35s are identified as cells with blue nuclei but without the red stain (A, B). F-actin staining was strong in areas with high concentrations of NHFs (I). Areas of H35s, not in contact with NHFs, had a weak f-actin signal (II). H35s in contact with NHFs have a distinctly strong f-actin signal (III). (B) Higher magnification of region (III) shows a strong f-actin signal located at the junction of an NHF and surrounding H35s. The f-actin signal continues to the nuclei of H35 cells. Scale bars are 20 μm.

SI Table 3-1: The shapes of NHFs and the differences in the elastic moduli of the two cell types determine the enhancement of stress in heterotypic mixes. The elliptic shapes are characterized by the ratio of the major axis (a) to the minor axis (b). All the stresses are normalized by the Young's modulus of NHFs (2 kPa). Stress enhancement equals the ratio of stresses in heterotypic environments to the stresses (0.0035) in homotypic NHFs located close to the periphery of the torus.

NHF Shape	Average Tensile Stress in the NHFs	Stress at Center of the Surrounding H35s	Stress Enhancement in the NHFs
Round	0.0053	0.0019	1.5X
Ellipse (a/b=2)	0.0069	0.0012	2.0X
Ellipse (a/b=5)	0.0084	0.0009	2.4X
Ellipse (a/b=5) and stiffness 5:1 (H35:NHF)	0.0125	0.0042	3.6X

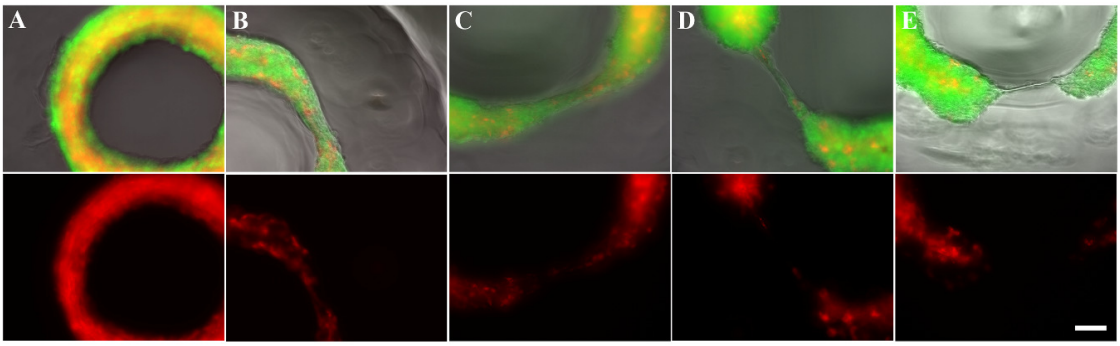

SI Figure 3-4: Heterotypic toroids are under tension and are necking after 24 hours. NHFs and H35s labeled red and green, respectively, were seeded at NHF: H35 ratios of 1:4 (A), 1:6 (B), 1:10 (C), 1:16 (D), and 1:20 (E). The top row shows the morphology of both the NHFs (red) and H35s (green). The bottom row shows the NHFs alone within the heterotypic toroid. Both NHFs and H35s are stretched beyond their original length and are aligned with the direction of stress. Scale bar is 100 μm.

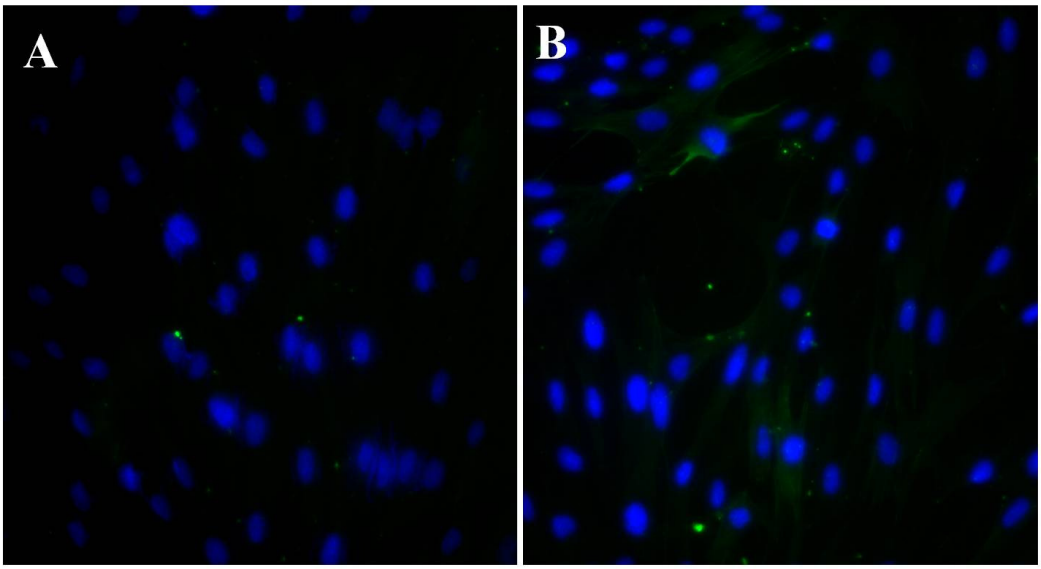

SI Figure 3-5: α-smooth muscle actin (α-SMA) expression was induced in NHFs after TGF-β treatment. NHFs were treated with 5 ng/ml TGF-β for 48 hours, fixed, permeabilized, and stained using a monoclonal anti-α-SMA antibody and a FITC labeled secondary. NHFs treated with TGF-β (B) had a stronger α-SMA (green) then the untreated NHFs (A).

CHAPTER 4

4. Conclusions and Future Directions

This dissertation had three primary objectives: (1) To develop a systems biology approach to quantify the forces involved in the self-assembly of cells into microtissues. (2) To quantify the contribution of active cellular contraction to the self-assembly of cells into microtissues. (3) To quantify the forces involved in the self-assembly of microtissues that contain more than one cell type (mixed or heterotypic microtissues). These goals were created so that cellular contraction and mechano-transduction could be studied in a 3D environment in which cell-cell interactions dominate.

Chapter 1 provided a review of cellular contractile forces. The chapter discussed the role of cellular contraction in embryogenesis, morphogenesis, wound healing, and in the differentiation of the fibroblast into the myofibroblast. Also reviewed are the different 2D and 3D assays that have been developed for measuring contractile forces as well as the reductionist approaches used to measure the forces and energies of some of the proteins involved in cellular contraction. The chapter also outlined the limitations of current methods to look at cellular contraction and the need for a 3D systems biology approach to measure cellular forces and energies when cell-cell interactions are maximized. As well,

complex shaped self-assembled microtissues were identified as a unique model for studying cellular forces.

In Chapter 2, a novel assay to measure cellular mechanics was described. The assay is based on the phenomenon that mono-dispersed cells, seeded into toroid shaped recesses, ascend the cone shaped hydrogel peg. The rate of upward motion, in addition to the weight of the microtissue gives a metric to measure the forces involved in the self-assembly of mono-dispersed cells into microtissues. This assay is completely non-contacting, non-invasive, straightforward, and requires no instrument calibration. Additionally, this assay provides a systems biology approach to measuring all of the cellular components that contribute to the power generation of the cells. Chapter 2 demonstrated how the assay is useful for comparing cell types. Although the chapter only describes the work done with two cell types, NHFs and H35s, the cell power for a number of different cell types including a glial blastoma cell line (C6), a breast cancer cell line (HS578Ts), and an ovarian granulosa cell line (KGNs) have been measured (**Appendix A, Figure A-2 and Table A-2**). Each of these cell types moved at different rates and had a unique power profile demonstrating the usefulness of the assay at comparing and characterizing cell types. Interestingly, using these cell types we hypothesized different stages that occur as the cells exert cell power, and each of these stages may be controlled by a different cellular mechanism (**Appendix A, Figure A-3)**.

Chapter 2 also showed how the assay is useful for modulating the effect of gravity, by changing cone slope, and also for teasing out the role of ROCK mediated cellular

contraction. The assay demonstrated the importance of ROCK mediated contraction in the self-assembly of both highly contractile fibroblasts as well as the non-contractile H35s. Using the cell power assay we also demonstrated that not only can cell power be slowed down, but it can also be increased as shown in the TGF-β experiments described in Chapter 3. This further demonstrated the importance of cellular contraction in cell-cell adhesion. Although unreported in Chapter 2 or 3, we also showed that other cellular components could be targeted using the cell power assay. Besides ROCK mediated contraction, we also looked at the contribution of microtubules to the self-assembly process (**Appendix A, Figure A-4**)

Giving relevance to tissues containing more than one cell type, Chapter 3 examined the cell power of mixed microtissues. We established that cellular forces in 3D tissues containing more than one cell type could be measured using cell power and we identified the importance of heterotypic cell interactions in increasing cellular force generation with our enhanced power measurements. We foresee this enhanced power assay to be useful for looking at a number of applications in which cell-cell heterotypic interactions may be important such as fibrosis and metastasis.

Despite the importance and usefulness of this assay, there are still some limitations. First, like many of the assays developed to look at cellular mechanics, this assay calculates cell power by simply dividing toroid power by the number of cells present. As previously described, this is not entirely accurate because cells are known to exert forces based on location and since the cells are pulling in multiple directions, which results in force cancellation. Second, since this assay is a power measurement (work/time) and not just pure force, it does not account for the exerted forces that do not result in work, i.e. displacements in the x dimension. So once again, power is only a lower limit of the energy and forces of the cells as they self-assemble.

4.1. Cell Power and Toroid Microtissues as an Anti-fibrotic Drug Screening Platform

In many tissues subject to fibrosis, including the liver, heart valves/leaflets, lungs, and kidney there is an increased population of myofibroblasts. These cells, key to wound healing, over populate the tissue leading to the eventual destruction of the parenchyma and the stiffening and scaring of the organ. In healthy wound healing, when the tissue sustains an injury either resident fibroblasts or circulating fibroblasts migrate into the wound and then differentiate into myofibroblasts. Myofibroblasts are highly contractile fibroblasts which synthesize and release proteins and growth factors to aid in the healing process. In healthy wound healing, the action and population of the myofibroblasts desists and the tissues function is restored. In chronic, uncontrolled wound healing, the population of myofibroblasts persists. These cells over populate the tissue with collagen I and exert unhealthy amounts of tension which further exacerbates the situation, as the increased tension initiates the differentiation of more fibroblasts into the highly active myofibroblast phenotype (1).

The cell power assay may be a useful platform for studying anti-fibrotic therapies. In Chapter 3, we discussed the enhanced power that is in both NHF/H35 and NHF$^{TGF-\beta1}$/H35 microtissues. Based on the enhanced cell power and the stress modeling, we hypothesize that these microtissues may be a good model for a liver tissue that would be more likely to develop fibrosis. Due to the enhanced power, the cells are under quite a different mechanical environment with increased tension. Specifically, if the enhanced

power is distributed among NHFs, these NHFs are 22x more powerful than when NHFs only have homotypic interactions. If the excess power is distributed among the H35s, the H35s, a cell type that has very little power, are just as powerful as fibroblasts (our most powerful cell type). Either of these scenarios, or a combination of the two, would lead to an incredibly different tension environment for the parenchymal cells of the liver as confirmed by our stress modeling. Such a great change in the mechanical environment of the liver could lead to either the myofibroblasts becoming overactive or the hepatocytes becoming myofibroblastic (type II epithelial to mesenchyal transition; EMT) both of which could promote fibrosis (2, 3).

Cell power could be a tool to measure a microtissue's pre-fibrotic potential and as a screen for anti-fibrotic therapies. The main parameter that would indicate pre-fibrotic potential is the enhanced power. Enhanced power is a quantitative measure of the disruption or change that has occurred in a tissue's mechanical environment. Experimentally, we could take measurements for the cell power of pure H35 microtissues to get a baseline value for homeostatic tension (as measured by cell power) in liver tissues. Then we would create our pre-fibrotic tissues, which in the case of the liver would be the $NHF^{TGF-\beta}$ /H35 microtissue, and measure the enhanced power in these tissues. To use these microtissues as an anti-fibrotic drug screening tool, the pre-fibrotic microtissues would be treated with prospective drugs and then enhanced power would be measured again. Our hypothesis is if enhanced power is eliminated, then the mechanical tension would be restored to normal, thus decreasing the potential for fibrosis.

Using enhanced power we can quantify how different factors contribute to changes in the tension environment. Some factors that could be studied include the heterotypic environment (including the effect of different cell types and their ratio) and growth factors (TGF-β, HGF, VEGF etc). Here, we describe the assay as a liver model; however, this assay could be used from a number of tissues that are prone to fibrosis.

These 3D microtissues and the cell power assay could present many advantages over traditional fibrosis screening models. Little research is available about how cell-cell interactions promote fibrosis. Most of the research done in 3D has used collagen matrices in which cell-ECM interactions dominate. These microtissues present a 3D environment in which cell-cell interactions are maximized, and in addition to quantitative measures of cell power, these tissues are amenable for studying qualitative biomarkers.

4.2. Cell Power and Metastasis

Cell power measurements may also be useful for determining a cancer cell's metastatic potential or for studying the importance of epithelial/mesenchyal interactions in relation to cancer. About ten years ago, six "hallmarks of cancer" were identified. These hallmarks included: sustaining proliferative signaling, evading growth suppressors, resisting cell death, enabling replicative immortality, inducing angiogenesis, and activating invasion and metastasis (4).The last hallmark, activating invasion and metastasis, is highly dependent on the cell gaining a migratory phenotype. Cell power may be a useful indicator of migration and thus how invasive the cell may be (5). For example, in the case of tumors derived from epithelial cells, another key to the cells becoming more invasive is the transitioning of the cells towards a mesenchymal phenotype (type III EMT) (6). This is marked by the cell having a rearranged cytoskeleton and a change in cadherin expression. In our heterotypic $NHF^{TGF-\beta}$/H35 microtissues, we noticed enhanced power, changes in cyotskeletal arrangement, and more mixing (less sorting), which may be an indication of changes in cadherin expression. These changes were attributed to changes in the tension environment and therefore were assumed to be a good model for fibrosis. However, these changes in the microtissue may be a model for cancer cell invasion. Enhanced power and the decrease in cell sorting may be an indication of how invasive and how likely the cell may be to metastasize.

The cone assay may also be useful for comparing the cell power of different known cancer cell lines. For example, there are a number of breast cancer lines with known metastatic potential. By measuring the cell power of these cell lines, a correlation

between metastatic potential and cell power could be developed. Also, stromal cell interactions have been demonstrated to be very important in cancer cell biology (7). These 3D microtissues present an environment where epithelial/stromal cell interactions could be studied. Using the assay, we could examine the role of heterotypic cell interactions, enhanced cell power, protein expression, and cell invasion. Additionally, the importance of growth factors such as TGF-β, HGF, PDGF, and VEGF could be examined in terms of cell power. If a correlation is developed between cell power and cell invasion, then the assay could also be used as a drug screening platform.

4.3. References

1. Hinz B (2009) Tissue stiffness, latent TGF-beta1 activation, and mechanical signal transduction: implications for the pathogenesis and treatment of fibrosis. *Curr Rheumatol Rep* 11(2):120-126.
2. Guarino M, Tosoni A, & Nebuloni M (2009) Direct contribution of epithelium to organ fibrosis: epithelial-mesenchymal transition. *Hum Pathol* 40(10):1365-1376.
3. Novo E, di Bonzo LV, Cannito S, Colombatto S, & Parola M (2009) Hepatic myofibroblasts: a heterogeneous population of multifunctional cells in liver fibrogenesis. *Int J Biochem Cell Biol* 41(11):2089-2093.
4. Hanahan D & Weinberg RA (2000) The hallmarks of cancer. *Cell* 100(1):57-70.
5. Pietras K & Ostman A (2010) Hallmarks of cancer: interactions with the tumor stroma. *Exp Cell Res* 316(8):1324-1331.
6. Kalluri R (2009) EMT: when epithelial cells decide to become mesenchymal-like cells. *J Clin Invest* 119(6):1417-1419.
7. Franco OE, Shaw AK, Strand DW, & Hayward SW (2010) Cancer associated fibroblasts in cancer pathogenesis. *Semin Cell Dev Biol* 21(1):33-39.

APPENDIX A

To determine if the cell power assay could be expanded to other cell types we conducted the cone assay for a breast cancer cell line (HS578Ts), an ovarian granulosa cell line (KGNs), calf pulmonary artery endothelial cells (CPAEs), and a glial blastoma cell line (C6s). We measured the density and the diameter of each cell type (**Table A-1**). We then seeded the cells into 65° toroid recesses at 20,833 cells per well and then measured the height of the toroids every two hours for eight hours and at 24 hours. Each of the cell types began moving up the peg at different times and reached different heights (**Figure A-1**). From the height of the microtissue and the weight, we calculated the cell power for each of the cell types (**Figure A-2**). We also examined the motion of CPAEs which did not begin to move until 24 hours. However, because of the small cell diameter of the CPAEs, many of the samples failed and so we did not have a significant sample size to compare the cell power of these cells. In terms of cell power, the cells rank as NHF, HS578T, C6, KGN, and H35 as the most to least powerful cell type (**Table A-2**).

From observing the power profiles of the different cell types (**Figure A-2**) it appears that within the eight hours each of the cell types were in different "stages" of power output and that each cell type follows a set pattern for producing power (**Figure A-3**). There is an initial increase in power (A) followed by a stage in which power is constant (B) and finally a steady decrease in power (C). We believe that each cell type goes through each

stage, but the duration of each stage, and the point at which each cell type reaches each stage varies. For example, when power is measured for the NHFs at two hours, they have already passed the rapid increase in power (stage A) and constant power (stage B), and have already entered into stage C. C6s, on the other hand, enter into stage A at two hours, stage B at six hours, and have not left this stage at eight hours.

For each of these stages we can also predict a mechanism for power generation. When a cell is exposed to trypsin, the majority of its binding proteins are removed from the cell surface. As the cells continue to restore these proteins to the cell's surface (the duration of stage A) there becomes a very large unfullfilled binding potential for the cells. The filling of these bonds, in addition to the generation of more unfullfilled bonds on the cell surface, leads to a great increase in power as seen in stage A. Also, the cells begin to exert contractile forces on each other and the peg causes stresses within the cells. These stresses lead to more actin recruitment, more contractility, and thus more power. After the rapid production of binding proteins and the force exertion in stage A, the cells enter into a stage in which the rate at which they produce surface binders is the same as which they are being filled (stage B), and results in a steady output of power. Once the production of binding proteins has ceased, there is a period of surface area minimization in which power is generated, but is slowing, as there are fewer and fewer unbound surface proteins (stage C). In addition, a homeostasis in contractile force generation is achieved resulting in a slowing in cell power.

To determine if the cell power assay could be used to determine the contribution of other protein systems to the self-assembly process we chose to look at the role of microtubules in the self-assembly of NHFs. Prior to seeding into toroid recesses, NHFs were treated with 10 μM paclitaxol, which stabilizes microtubules, and cell power was measured every two hours for eight hours. Compared to the controls, the height of the paclitaxol treated NHF toroids was substantially reduced as early as two hours and continued to be less for the duration of the experiment (**Figure A-4**). This change in cell height corresponded to an overal 38 $\pm$ 4.7% reduction in cell power, indicating the importance of cell stiffness in power generation. Cellular stiffness was not measured, nevertheless, these data indicates that if a cell is stiffer it may not be able to as effectively use its power against gravity.

Appendix A: Figures

Table A-1: The density, diameter, volume, and surface area of various cell types.

Cell Type	Density (g/cm^3)	Diameter (μm)	Volume (μm^3)	Surface Area (μm^2)
C6s	1.07	15	1832	723
CPAEs	1.03	15	1615	665
KGNs	1.04	20	4092	1236
H35s	1.08	17	2572	907
HS578Ts	1.03	21	4765	1368
NHFs	1.05	20	4188	1256

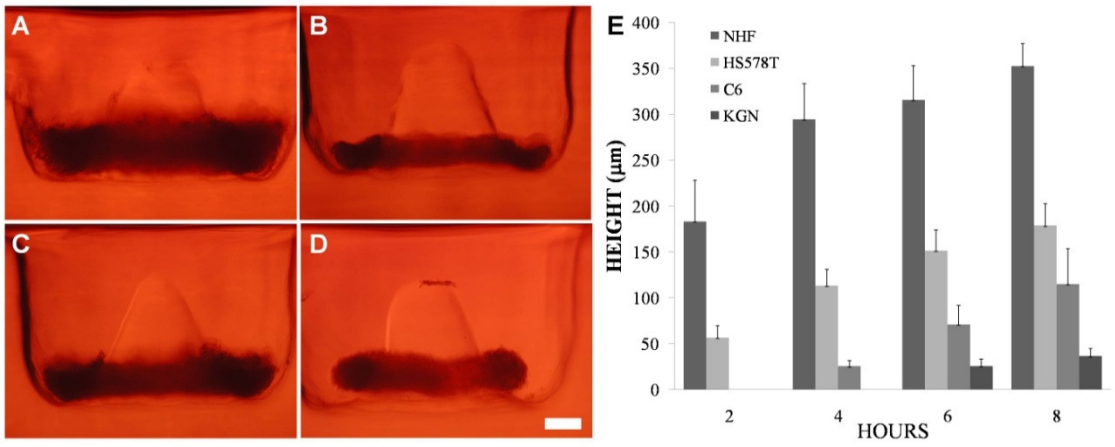

Figure A-1: Cell types vary in the rate in which they move up the conical peg. HS578Ts (A), C6s (B), KGNs (C) and CPAEs (D) began to move up the peg at 2, 4, 6 and 24 hours, respectively. The height of the microtissues was plotted over 8 hours (E). CPAE samples did not begin moving until 24 hours and many of the samples failed, so height was not measured.

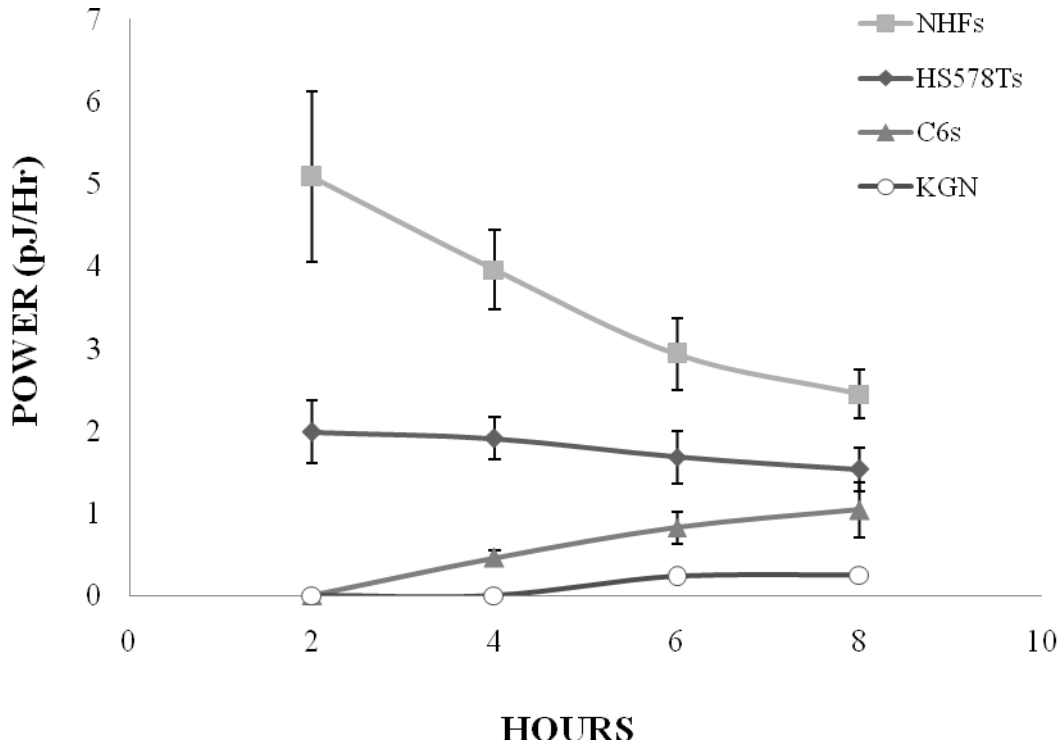

Figure A-2: Power output differed for each cell type. NHFs (square), HS578Ts (diamond), C6s (triangle), and KGNs (open circles) all began to output power at different times and at different magnitudes.

Table A-2: Peak Power values and times for each cell type

Cell Type	Peak Power (fJ/hr per cell)	Time (hrs)
NHF	.24 $\pm$. 05	2
HS578T	.10 $\pm$. 02	2
C6	.08 $\pm$. 02	8
KGN	.03 $\pm$. 01	6
H35	.02 $\pm$. 004	24

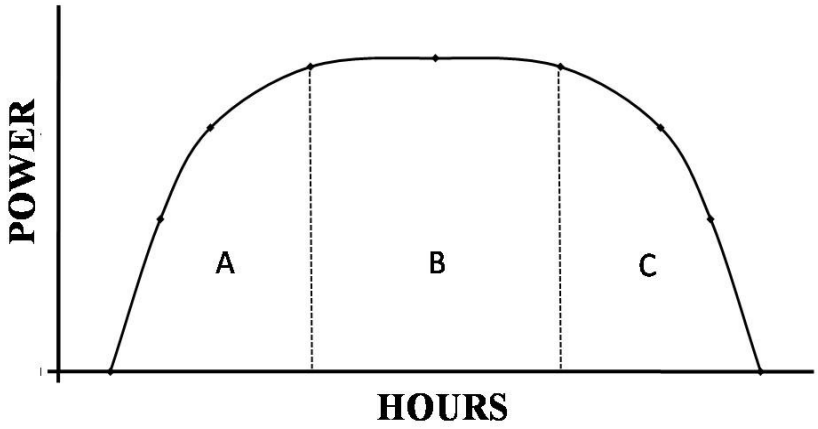

Figure A-3: Schematic of the proposed power profile for cell types. As the cells self-assemble they first enter into a stage in which they rapidly are producing binding proteins (A). With this rapid production is also a rapid fulfilling of these bonds which results in a great increase in power. As the bonds are being filled, the rate at which they are produced matches that which they are occupied resulting in a steady output in power (B). After binder production has ceased, the remaining bonds get filled until power reaches zero (C).

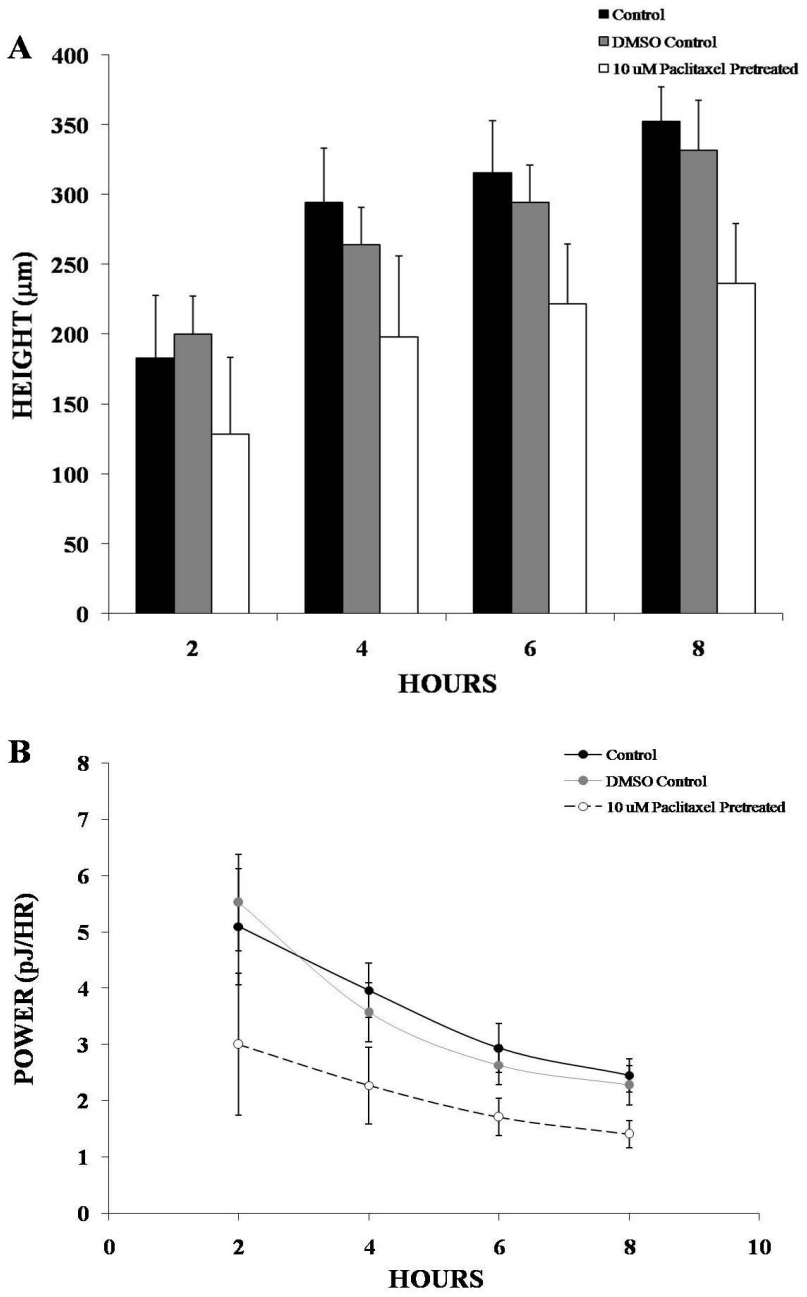

Figure A-4: Stabilizing microtubules reduced cell power by 38%. NHFs were treated with 10 µM paclitaxol and cell power was measured. The height (A) of the treated microtissues (white) was significantly reduced compared to the untreated samples (black) and the vehicle control (gray). Cell power (B) was not changed between the untreated and vehicle controls (black and gray, respectively) but was reduced with the stabilization of microtubules.